Heat-treated optimized polysulfone electrospun nanofibrous membranes for high performance wastewater microfiltration

P. Arribas[1,2,*], M.C. García-Payo[2], M. Khayet[2,3,*], L. Gil [4]

[1]Campus of International Excellence, Moncloa Campus (UCM-UPM), Madrid (Spain).

[2]Department of Structure of Matter, Thermal Physics and Electronics, Faculty of Physics, University Complutense of Madrid, Avda. Complutense s/n, 28040, Madrid (Spain).

[3]Madrid Institute for Advanced Studies of Water (IMDEA Water Institute), Calle Punto Net Nº 4, 28805, Alcalá de Henares, Madrid (Spain).

[4]Genetics and Eco-Physiology Research Group, School of Forest Engineering, University Polytechnic of Madrid, Avda. Complutense s/n, 28040, Madrid (Spain).

* Corresponding authors: khayetm@fis.ucm.es; paulaarribas@ucm.es

Tel. +34-91-3944448; +34-91-3945185

Fax. +34-91-3945191

Graphical Abstract

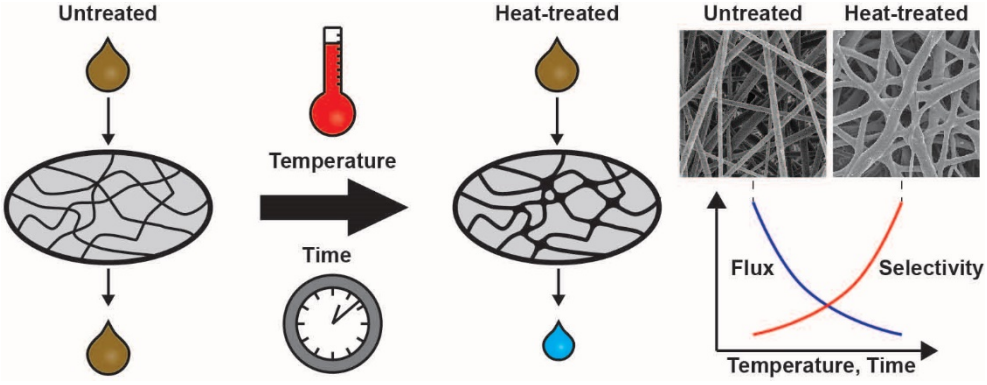

Abstract

The structure and morphology of self-sustained electrospun nanofibrous membranes (ENMs) are key factors determining membrane performance for filtration applications. In this study, heat post-treatment (HPT) method was applied to modify the structural and morphological properties of polysulfone (PSU) ENMs, to improve their filtration performance and to obtain membranes suitable for wastewater treatment. The influence of the HPT temperature and time on the morphological structure of the PSU ENMs as well as on fouling and filtration performance was investigated. Microfiltration (MF) tests were conducted using humic acid model solutions with a concentration of 15 mg/L at pH 11. Increasing the HPT temperature or time, led to an increase of the mean nanofiber diameter along with a decrease of the mean size of the inter-fiber space, the void volume fraction and the water contact angle. ENMs treated with a higher HPT temperature and a longer time exhibited higher nanofibers interconnectivity and a more compact structure with a smaller size of inter-fiber spaces. Under the same MF operating conditions, a commercial polyethersulfone (PES) MF membrane (HPWP, Millipore) had lower filtration performance (i.e. lower performance index, *PI*, 82 kg/m^2.h) than the treated-optimized PSU ENMs (i.e. 147 and 133 kg/m^2.h for ENMs 9 and 10, respectively). The obtained results confirm the good performance of the developed PSU ENMs for MF applications.

Keywords: Nanofiber; Heat post-treatment; Electrospun membrane; Humic acid; Microfiltration.

1. Introduction

The development of efficient membrane filtration technologies is especially important as water shortage has become a growing global problem in recent years [1]. The improved compactness, low cost operation, high energy efficiency and high throughput enable membrane separation processes to compete successfully with conventional separation processes. In fact, membranes are an environmentally-friendly method highly utilized in waste treatment, water purification and in clarification and concentration processes [2]. However, the fabrication of adequately designed membranes for a specific application is challenging [3]. Electrospinning is an attractive and efficient technique for polymer solution processing that provides a simple and versatile way to prepare ultrafine polymeric fibers with micro- to nano-scale diameters, ranging from 50 nm to 10 μm thickness [4, 5]. Electrospun fibers are typically collected in the form of a non-woven mesh, which is of importance for a variety of applications including semi-permeable membranes, filters, composite reinforcement and scaffolding used in tissue engineering [6]. Electrospun nanofibrous membranes (ENMs) have a great potential for membrane filtration due to their attractive structural features, such as high porosity and interconnected open pore structure, micro-scale interstitial space, controllable thickness and a large surface area to volume ratio [7]. In ENMs the pores are induced by the entanglement of interconnected nanofibers (i.e. inter-fiber space). The mean pore size of ENMs correlates with the nanofiber diameter [8]. Thus, the pore size of ENMs can be tuned to meet different filtration requirements by changing the nanofiber diameter.

Advantages of using ENMs for water treatment include high permeability, mainly related to their high void volume fraction (i.e. porosity), and good separation factor due to the highly tortuous path through the nanofibrous structure and the remaining static

charge in the nanofibers after electrospinning, which helps to separate different contaminants [9-11]. In recent years, Microfiltration (MF) has attracted increasing attention in the field of wastewater treatment and reclamation as an alternative to conventional water treatment processes (i.e. coagulation, sedimentation and sand filtration) [12]. MF offers several advantages including easier control of operation, and reduced maintenance and sludge production. However, a major factor that limits the use of membranes in water treatment is membrane fouling, which reduces water production rates and increases energy consumption [13]. Fouling reduces the effective membrane surface for filtration leading to a strong decline of permeate flux and worse separation performance [7, 14, 15]. Given that membrane properties have a high impact on fouling, it is important to understand their effects well in order to develop adequate membranes that are capable to mitigate fouling. For instance, it has been demonstrated that membrane hydrophobicity, roughness, pore size and pore morphology affect membrane-foulant-interactions and consequently, fouling effects [16].

In the literature, there is a large number of studies using nanofibrous scaffolds or ENMs as pre-filters for particulate removal through MF/UF applications. One of the most mentioned drawbacks of ENMs is the low mechanical strength and the difficulty of handling them after electrospinning [17]. Several methods were proposed to overcome these problems before their application in filtration: plasticization [18]; polymer blending [19]; solvent induced inter-nanofiber bonding [9]; hot-pressing [20-22]; heat treatment [5-7, 23-26]; addition of nanoparticles [27, 28]; use of crosslinking agents [29]. One of the most effective approaches is to enhance the bonding at junction points in the nanofiber mat by welding the nanofibers together, as for example by applying a heat post-treatment (HPT) (i.e. heating the mat between the glass transition temperature of the electrospun polymer and its melting temperature). Compared to plasticizing and polymer blending,

99 an appropriate heat treatment may be more environmental friendly and less energy
100 consuming. The incorporation of nanoparticles in the membrane matrix, such as titanium
101 dioxide, usually needs a post-treatment of the membrane (e.g. hydrothermal bath,
102 annealing), which increases the membrane fabrication costs [27]. Moreover, although
103 hot-pressing has been reported to increase the structural integrity and mechanical strength
104 of the ENMs, heat treatment can also induce a change in the molecular structure of the
105 polymer, leading to a higher degree of nanofibers crystallinity [30] and, consequently, to
106 a greater elastic modulus of the ENMs [2, 23].

107 In this study, the filtration properties of polysulfone electrospun nanofibrous
108 membranes (PSU ENMs) were improved by the application of HPT. The effects of the
109 HPT temperature and the HPT time on the structural and morphological properties of the
110 membranes (i.e. porosity, pore size and its distribution, wettability, thickness) were
111 investigated, because these factors affect the membrane filtration performance [2, 31].
112 The filtration performance index (*PI*) was considered to select the optimum heating
113 conditions for the application of the ENMs in wastewater treatment by MF.

114 ## 2. Materials and methods

115 ### 2.1. Materials

116 The polymer polysulfone (PSU, UDEL P-3500 LCD, Solvay Specialty Polymers; Mw
117 = 79,000 g/mol; ρ = 1.24 g/cm^3) and the mixture of solvents N, N-dimethyl formamide
118 (DMF, Sigma-Aldrich) and tetrahydrofuran (THF, Sigma-Aldrich) were used to prepare
119 the spinning solution. The organic foulant humic acid (HA, Fluka) with a molecular
120 weight of 4.1 kDa was utilized to prepare the feed solution for the MF tests. Sodium
121 hydroxide (NaOH, Panreac) was used to prepare a concentrated HA stock solution of 1
122 g/L. Hydrochloric acid (HCl, Sigma-Aldrich) was employed to adjust the pH of the
123 diluted HA feed solutions (15 mg/L) to 11. Isopropyl alcohol (IPA, Sigma-Aldrich) was

used to determine the void volume fraction (ε) of the PSU ENMs. POREFIL®, a fluorinated hydrocarbon (chemical nature: pefluoroether; surface tension: 16 mN/m, vapor pressure: 3.33 Pa; viscosity: 4.4 mPa·s, POROMETER) was used as a wetting liquid to perform the inter-fiber space measurements.

2.2.Preparation and characterization of the polymer solution

The polymer solution was prepared by mixing DMF (64 wt.%) and THF (16 wt.%) at room temperature with a magnetic stirrer (IKA, RCT basic) for 2 min at 80 rpm. Subsequently, 20 wt.% PSU was added to the solvent mixture and the solution was stirred at 60°C and 80 rpm for 10 h until the PSU was completely dissolved and the resulting polymer solution homogeneous.

The polymer solution was characterized by measuring its surface tension, viscosity and electrical conductivity. The surface tension of the spinning solution was determined at room temperature by the pendant drop shape analysis using an Optical Contact Angle Meter (CAM 200) and a stainless steel needle with an outer diameter of 1.825 mm. The volume of all drops was maintained constant at 16.08 ± 0.82 μL. The viscosity of the spinning solution was measured with a Digital Viscometer (Brookfield, Model DV-I+) in a cylindrical sample container and using the SC4-31 spindle at 30 rpm and a shear rate of 10.2 s^{-1}. The temperature of the spinning solution was maintained constant at 25°C by a thermostat (Techne, Model TU-16D). The electrical conductivity of polymer solution was measured at 25°C using a conductivity meter (CyberScan con11 Conductivity/TDS/°C, Eutech Instruments).

147 **2.3. Preparation of PSU ENMs**

148 PSU ENMs were prepared by electrospinning using the polymer solution indicated
149 in the previous section. The used electrospinning system was described elsewhere [7]. In
150 this study, all PSU ENMs were prepared under the previously obtained optimum
151 electrospinning parameter conditions: a polymer solution flow rate of 2.5 mL/h, an
152 electric voltage of 16 kV, a distance between the needle tip and the collector or air gap of
153 10 cm and an electrospinning time of 45 min [7]. The ambient conditions during
154 electrospinning fabrication were a temperature between 20-25°C and a relative humidity
155 in the range 38-41%.

156

157 **2.4. Heat post-treatment (HPT) of PSU ENMs**

158 The silky, fluffy and loose structure of the PSU ENMs complicated their handling
159 after the electrospinning step. In addition, it was observed that PSU ENMs without any
160 HPT were not useful for filtration application as the membranes were not capable to
161 achieve any separation. Thus, a HPT step was carried out to get membranes with
162 improved structural integrity and greater filtration performance.

163 The HPT was carried out in a ceramic oven (CWF 13/13, Carbolite®). Before being
164 placed into the oven, the ENMs deposited on the aluminum foil were attached to a smaller
165 rounded copper support to avoid shrinkage of the membrane during heating. The samples
166 were first heated from 70°C to the established HPT temperature (i.e. 190- 250°C) at a rate
167 of 30°C/min (this process took between 6-8 min, depending on the final temperature) and
168 then exposed to the HPT temperature for a specific HPT time (i.e. 20-300 min). HPT
169 temperatures above the boiling point of the used solvents were chosen to guarantee their
170 complete evaporation from the formed ENMs. To induce good bonding points between
171 nanofibers (i.e. points in which nanofibers were fused together) the applied temperatures

were also higher than the glass transition temperature of the used polymer (185°C for PSU). After the HPT step, ENMs were wetted with DI water, peeled off from the aluminum foil, dried at room temperature for 24 h and stored until use.

In order to perform a systematic and accurate study on the effect of the HPT on the morphological structure of PSU ENMs, all membranes were obtained from the same manufacturing batch, avoiding as many steric dissimilarities (in terms of, for example, pore size, structure, porosity and surface roughness) between them as possible. In addition, SEM images of membranes with an initial thickness of 900 ± 50 μm were used to select those ENMs with similar initial nanofibrous structure (i.e. uniformity of the nanofiber web).

It was observed that not all the heat post-treatments (HPTs) led to the same morphology and structure of the membranes. In order to fully understand the influence of the applied HPT on the morphological and structural changes of PSU ENMs, a preliminary study with 90 membranes and 30 different HPTs was conducted to determine the operational working area (i.e. region of interest) of the HPT as shown later on. Then, a systematic study in this region of interest was conducted and eleven PSU ENMs were evaluated and compared in terms of their morphological characteristics (i.e. mean nanofiber diameter, mean size of the inter-fiber space, water contact angle, void volume fraction, etc.). Moreover, MF tests were carried out with these eleven ENMs to determine the optimum region of the HPT, in which the treated membranes exhibit the highest filtration performance indexes.

2.5. Characterization of PSU ENMs

The thickness of each PSU ENM was measured at 40 different spots on the sample using a micrometer equipped with a feeler (ISL Isocontrol). The final thickness of each

sample was determined as the average value of the measured thicknesses with its corresponding standard deviation.

The morphology of the surface of the PSU ENMs was evaluated with a field emission scanning electron microscope (FESEM, JEOL Model JSM-6335F) operating at 5 kV. Before conducting the SEM analysis, a thin gold layer of approximately 5 nm was sputter-coated on the membrane surface using an evaporator (EMITECH K550 X) for one minute under 25 mA. SEM images were analyzed with the UTHSCSA Image Tool 3.0 software to determine the nanofiber diameter. For each membrane, at least 3 SEM images were analyzed and the diameters of a total number of 100 nanofibers/per image were measured. Statistical analyses were applied to determine the nanofiber diameter distribution (i.e. nanofiber diameter histogram). The weighted arithmetic mean of the nanofiber diameters (λ_w) along with its corresponding weighted standard deviation (s_w) were evaluated as follows:

$$\lambda_w = \lambda_0 + \frac{h}{N}\sum_{j=1}^{m} u_j \cdot FC_j \tag{1}$$

$$s_w = \sqrt{\left(\frac{1}{N}\sum_{j=1}^{m}\left(u_j^2 \cdot FC_j\right) - \left(\frac{1}{N}\sum_{j=1}^{m}\left(u_j \cdot FC_j\right)\right)^2\right) \cdot h^2} \tag{2}$$

where m denotes de number of bins (disjoint categories), h is the width, $h = (\lambda_{max} - \lambda_{min})/m$, FC is the frequency count, N is the number of samples in the statistical set (in our case N = 100), λ_0 is the dominant characteristic of the statistical set that corresponds to the highest peak, u is a variable defined as $u = (\lambda_c - \lambda_0)/h$ and λ_c is the bin characteristic (or bin center).

The final value of the weighted arithmetic mean of the nanofiber diameters ($\overline{\lambda_w}$) with its corresponding weighted standard deviation ($\overline{s_w}$) for the PSU ENMs was determined

as the arithmetic mean and standard deviation of all SEM samples evaluated for each membrane.

The water contact angle (θ_w) values on the surface of the PSU ENMs were measured at room temperature using a computerized optical system (CAM100 device, Sb) equipped with a CCD camera and an image analysis software (Cam200usb). This system enables the acquisition of photographs of the water drop on the sample surface and to evaluate the contact angle. A Hamilton stainless steel needle was used to control the volume of the drops, which was between 12 and 14 μL. Every drop was recorded taking five images within 4 s. For each ENM sample at least 10 different drops were considered to determine the final averaged θ_w value together with its standard deviation.

The void volume fraction (i.e. porosity, ε) is defined as the ratio between the volume of the inter-fiber space and the total volume of the membrane. The value of ε was determined by measuring the density of the polymer material (ρ_{pol}) using isopropyl alcohol (IPA), which penetrates inside the inter-fiber space, and the density of the membrane (ρ_m) using distilled water, which does not get into the inter-fiber space, according to equation (3) [32].

$$\varepsilon\ (\%) = \left(1 - \frac{\rho_m}{\rho_{pol}}\right) \cdot 100 \qquad (3)$$

The inter-fiber space (d_f) of the PSU ENMs was measured with capillary flow porometry (CFP) using a gas–liquid displacement Porometer (POROLUX™ 100, Porometer). CFP uses the displacement of a wetting liquid inside a porous network by means of an inert gas flow to measure d_f. In this study, POREFIL® (Porometer) was used as the wetting liquid agent, compressed air was employed as the inert gas and the applied hydrostatic pressure was varied in the range of 0–0.7 MPa at room temperature (~23°C). The ENMs were first wetted by the POREFIL® and the gas permeation flow was

measured by increasing the transmembrane pressure to obtain the *S* shaped wet curve. Subsequently, the dry curve was obtained by measuring the gas flow through the dry sample as a function of the applied pressure. Both, the wet and dry curves were used to determine the mean size of the inter-fiber space ($\overline{d}_f$, which corresponds to the size of the inter-fiber space at which the wet curve intersects the half-dry curve that corresponds to 50% gas flow through the dry membrane), the inter-fiber space distribution or differential filter flow (*DFF*, which represents the increase in flow rate per unit increase in inter-fiber space), and the cumulative filter flow distribution (*CFF*, i.e. percentage of the total gas flow that goes through inter-fiber spaces of a certain size and larger) of the PSU EMNs.

2.6. Filtration experiments

The experimental set up used for MF tests was described elsewhere [7]. The effective filtration area of the membrane was (21.76 ± 0.01) 10^{-4} m^2. The feed solution was kept at room temperature (~23°C) and the feed flow rate was maintained at 1.6-1.8 L/min.

To carry out the MF tests, diluted HA feed solutions of 15 mg/L were prepared from a concentrated HA stock solution of 1 g/L. In our previous study, it was demonstrated that PSU ENMs were not selective to HA in acidic media (pH = 3), whereas clear HA separation factors were observed when using alkaline HA solutions (pH = 11) [7]. Thus, in this study the solution pH was adjusted to 11 by adding 2 M NaOH as needed using a pH/Ion meter (692, Metrohm). A spectrophotometer (UV/VIS 7315, Jenway) was used to determine the HA concentration of the permeate, the retentate and the feed samples at a wavelength of 254 nm.

Before carrying out the MF tests, all membranes were pre-compacted by circulating distilled water at a transmembrane pressure (ΔP) of 3 10^5 Pa for 3 h. Subsequently, MF tests were conducted at a transmembrane pressure of 10^5 Pa using first distilled water for

1 h to determine the pure water permeability (*PWP*), then the aqueous HA feed solution for 7 h (i.e. HA test), and finally distilled water again for 1 h. The permeate fluxes of both HA solution (J_{HA}) and distilled water before (J_{w_0}) and after (J_{w_f}) each HA test were measured and the irreversible fouling factor (FR_W) of the membrane was evaluated as follows [33]:

$$FR_W(\%) = \frac{J_{w_0} - J_{w_f}}{J_{w_0}} \cdot 100 \quad (4)$$

The permeate fluxes were calculated using the weight of the permeate produced during a specific time on an electronic balance (AND GF-1200) as follows:

$$J\left(\frac{kg}{m^2 h}\right) = \frac{m}{A_{ef}\Delta t} \quad (5)$$

where m is the mass of the obtained permeate over a period of time Δt and A_{ef} is the effective filtration membrane area.

The separation factor (α) of the membranes was evaluated using the following equation:

$$\alpha\ (\%) = \left(1 - \frac{2C_p}{C_r + C_f}\right) \cdot 100 \quad (6)$$

where C_p, C_r and C_f are the HA concentration of the permeate, retentate and feed solutions, respectively.

The initial HA permeate flux decline (FD_0), which relates to the beginning of the fouling of the membranes, was determined as follows:

$$FD_0 = 1 - \frac{J_{HA_0}}{J_{w_0}} \quad (7)$$

where J_{HA_0} corresponds to the HA permeate flux at the beginning of the filtration test.

The filtration performance of the membranes was evaluated considering the performance index (*PI*), which takes into account the final values of both the HA

permeate flux (J_{HA_f}) and the HA separation factor (α_f) obtained at the end of the HA test (after about 420 min of experiment):

$$PI(kg/m^2h) = \frac{J_{HA_f} \cdot \alpha_f}{100} \quad (8)$$

3. Results and discussions

3.1. Polymer solution characterization

The surface tension of the PSU electrospun solution is 35.8 ± 1.8 mN/m, its viscosity is 485.3 ± 0.8 mPa·s and its electrical conductivity is 9.12 ± 0.15 μS/cm. Similar values for the surface tension (35.47 mN/m) and the viscosity (520 mPa·s) of the PSU dope solution (20% wt/v PSU in DMAC/acetone (9:1) mixed solvents) were reported by Yuan et al. [34] when preparing ultrafine PSU fibers by electrospinning.

3.2. PSU ENMs preparation and characterization

3.2.1. Preliminary evaluation of PSU ENMs prepared with different HPTs and determination of the region of interest of the HPT

A preliminary HPT study (see Fig. 1) was carried out to evaluate 90 membranes treated with 30 different HPTs in terms of damage, thickness homogeneity and degree of networking (i.e. quantity of bonding points between nanofibers) after the HPT. A visual criterion was used to evaluate the damage of the membranes due to the HPT (see Fig. S1 in SI), giving 0 points to membranes that were burned on most of the surface, 5 points to membranes with only few small burned spots or 10 points to membranes without any burned spot on the surface. The final thickness homogeneity of the membrane was evaluated by means of the relative error of the thickness ($E_r = (\Delta\delta/\delta) \cdot 100$), giving 0, 1.5, 3.5, 5, 6.5, 8.5 or 10 points to membranes with a relative error of the thickness between 40-100, 30-40, 20-30, 15-20, 10-15, 5-10 and 0-5%, respectively. Finally, SEM images of the PSU ENMs surfaces were used to evaluate the degree of networking and

interconnectivity of the PSU ENMs, giving 0, 2.5, 5, 7.5 or 10 points to membranes in which a percentage of nanofiber intersections bonding < 20, 20-40, 40-60, 60-80 and > 80%, respectively (see Fig. S2 in SI). The individual scores from the three evaluations were averaged to obtain a normalized score from 0 to 10 for each membrane. The scores of all membranes fabricated under the same HPT condition were averaged to obtain a single score for that condition.

Fig. 1 shows a three-dimensional representation of the average scores of the different HPTs. A region of interest for further investigation was identified (average score > 6, orange and red colors), which corresponded to (210°C, t > 250 min), (220°C, 65 < t < 180 min) and (230°C, 35 < t < 90 min). Eleven different HPTs within the region of interest were used to systematically study the effects of the HPT temperature and time on the morphology and structure of the PSU ENMs as well as on their filtration performance.

3.2.2. Effects of the HPT temperature and time on the morphology and structure of PSU ENMs

Table 1 summarizes the morphological characteristics of the eleven PSU ENMs treated with different HPTs. It must be pointed out that the HPTs used to treat the ENM 1 (210°C/60 min), ENM 2 (210°C/90 min) and ENM 3 (220°C/60 min) were not within the region of interest, but they were useful to systematically study the effects of the changes of the HPT temperature. Figs. 2-5 show the morphological and structural properties of the PSU ENMs prepared with the different HPTs. One of the main effects of the application of the HPT was the reduction of the thickness of the ENMs, which decreased from 900 to 80-380 μm, depending on the applied HPT.

The changes of the surface of the PSU ENMs when increasing the HPT temperature from 210 to 230°C can be observed in Fig. 2. For both 60 and 90 min of HPT time, an

increase of the mean nanofiber diameter ($\overline{\lambda_w}$) (see Table 1 and Fig. 4) and nanofibers interconnectivity was observed when increasing the HPT temperature, resulting in membranes with improved integrity and a more compact structure [1, 5]. The same morphological and structural changes (i.e. increase of $\overline{\lambda_w}$ and the number of interconnected nanofibers) were observed by Liang. et al. [25] on PVDF ENMs when increasing the applied heat treatment temperature from 150 to 160°C. The increase of $\overline{\lambda_w}$ is attributed to the shrinkage of the nanofibers at high temperatures [6, 23, 25].

By comparing the SEM images of 60 min of HPT time with those of 90 min (Fig. 2), it can be noticed that the effect of increasing the HPT temperature was stronger at higher HPT time. For instance, ENMs 4 and 11 resulted in larger values of $\overline{\lambda_w}$ (i.e. thicker nanofibers, see Table 1 and Fig. 4) and higher degree of networking than that of the ENMs 3 and 9, respectively. Furthermore, ENMs 4 and 11 have more and larger junctions between nanofibers compared with those of the ENMs 3 and 9.

As can be seen in Fig. 3, different increments of the HPT time (30 and 15 min) for the membranes treated at 220 and 230°C, respectively, were established to avoid burning the membranes, as the effects of increasing the HPT time on the structure and morphology of the membrane were notably stronger when the applied temperature was higher. In fact, the maximum applied HPT time without observing any burned spot on the membrane was 180 min at 220°C, twice as long as that for the membranes treated at 230°C (90 min).

No connection points between nanofibers could be detected on the surface of the membranes prepared with the lowest HPT times (ENM 3, 60 min at 220°C, and ENM 8, 45 min at 230°C). In these cases, the nanofibers were smaller in diameter (i.e. thinner nanofibers), cylindrical and curled. Similar nanofiber structures were also reported by Homaeigohar et al. [24] on polyethersulfone (PES) ENMs without heat-treatment.

When increasing the HPT time at 220 or 230°C, an enhancement of the degree of networking was observed and the nanofibers became thicker and flatter, resulting in membranes with a more compact structure. In addition, the inter-fiber spaces of the PSU ENMs, which were large and without any specific geometrical shape for low HPT times, became smaller with rounder edges when the HPT time was increased. For instance, the nanofiber network of the membrane prepared with the highest HPT time, 180 minutes at 220°C (see SEM image of ENM 7 in Fig. 3), had relatively small and rounded inter-fiber spaces together with more fused nanofibers. Similar membrane morphologies were also observed in electrospun poly (lactic acid) (PLA) membranes treated for 120 min at 90°C [26].

Increasing the HPT temperature from 210 to 230°C led to an increase of $\overline{\lambda_w}$ by 4.6 and 18.9%, respectively, for the applied HPT times of 60 and 90 min (Fig. 4A left). It is worth noting that increasing the HPT time by only 30 min, resulted in ~4 times greater enhancement of $\overline{\lambda_w}$ at the highest HPT temperature. A greater increase of $\overline{\lambda_w}$ was achieved by increasing the HPT time from 60 to 180 min at 220°C and from 45 to 90 min at 230°C (22.4 and 19.7%, respectively, Fig. 4A right). Furthermore, the nanofiber diameter distribution histograms of the PSU ENMs (Fig. S3 in SI) became broader when increasing both the HPT temperature and the HPT time as claimed by Liang et al. [25]. For example, the nanofiber diameter distribution of the ENM 7 treated at 220°C for 180 min (0.5 to 1.6 μm) was wider than that of the ENM 3 treated at 220°C for 60 min (0.3 to 1.2 μm).

A left shift of both the cumulative (*CFF*, Fig. 5A-B) and the differential (*DFF*, Fig. 5A-B) inter-fiber space distributions along with a decrease of the mean size of the inter-fiber space ($\overline{d_f}$) were observed. When the HPT temperature was increased from 210 to 230°C, $\overline{d_f}$ decreased by 15.5%, and when the HPT time was increased from 45 to 90 min,

389 $\overline{d_f}$ decreased by 18.7%. The detected reduction of $\overline{d_f}$ was mainly caused by the increase
390 of $\overline{\lambda_w}$ and the degree of networking (Fig. S4 in SI). The latter effect was also reported in
391 other previous studies [1, 26].

392 The obtained values of $\overline{\lambda_w}$ (from 690 ± 30 to 850 ± 40 nm) and $\overline{d_f}$ (from 2.6 to 3.3
393 μm) for all PSU ENMs in this study (Table 1) are comparable to those reported by both
394 Gopal et al. [3] for PSU ENMs treated at 188°C for 180 min (470 ± 150 nm; 2.1 μm) and
395 Lui et al. [35] for PSU ENMs treated at 190°C for 120 min (663 ± 254 nm; 4.5 μm).

396 It was expected that the changes in the size of the nanofibers and the inter-fiber spaces
397 of the PSU ENMs resulted in notable effects on the total void volume fraction and
398 permeation properties of the membranes [36]. In fact, a gradual decrease of both the void
399 volume fraction (ε) and the water contact angle (θ_w) of the PSU ENMs was observed with
400 the increase of the HPT temperature and time (Figs. 4B and C). The increase of the HPT
401 temperature from 210 to 230°C caused a reduction of ε by 13.2 and 15.7% when the
402 applied HPT time was 60 and 90 min, respectively (Fig.4B left). Meanwhile, a reduction
403 of ε by 19.9 and 15.4% was detected when the applied HPT time was varied from 60 to
404 180 min at 220°C and from 45 to 90 min at 230°C, respectively (Fig. 4B right). It is worth
405 noting that although t ε was reduced, it still remained sufficiently high (above 70%, see
406 Table 1). The values of ε of the prepared PSU ENMs ranged between 72.3 (ENM 7,
407 220°C/180 min) to 94.2% (ENM 1, 210°C/60 min), which is well within the range
408 reported for non-woven PSU ultrafine fiber mats treated at 188°C for 360 min (80-85%)
409 [5] and PVDF ENMs treated at 80°C for 30 min (85-93%) [37].

410 The reduction of θ_w of PSU ENMs (Fig. 4C) could be due to the gradual flattening of
411 the nanofibers when increasing the HPT temperature or time, resulting in smoother
412 membrane surfaces [38, 39]. Increasing the HPT temperature from 210 to 230°C at a HPT

time of 60 min decreased the values of θ_w from 137.4 to 125.7°; at a HPT time of 90 min it decreased the value of θ_w from 135.9 to 115.4° (Fig. 4C left). When increasing the HPT time from 60 to 180 min at 220°C θ_w was reduced from 135.0 to 120.4°, whereas by increasing the HPT time from 45 to 90 min at 230°C θ_w was reduced from 135.4 to 115.4° (Fig. 4C right). During the applied HPT, the hydrophobic character of the ENMs decreased reducing the membrane water contact angles by up to 15%. However, the surfaces of all heat-treated ENMs retained their hydrophobic character with contact angles θ_w >115° (see Table 1). Similar θ_w values were reported for PSU ultrafine ENMs heat-treated at 188°C for 360 min (135 ± 5°) [5]. It is to be noted that the hydrophobic character was also maintained in PVDF ENMs heat-treated at 120°C for 120 min (127.0 ± 1.1°) [40] and PVDF-HFP ENMs hot-pressed at 200°C for 2 s (125.0 ± 2.5°) [21].

All observed trends of the morphological characteristics ($\uparrow\overline{\lambda_w}$, $\downarrow\overline{d_f}$, $\downarrow\varepsilon$, $\downarrow\theta_w$) of the PSU ENMs when increasing the HPT temperature or time, correlated well with the changes of the surface and the morphology of the PSU ENMs (higher interconnectivity and more compacted structure), which were larger for the ENMs 7 and 11.

The SEM images and the morphological characteristics of the membranes treated at a HPT temperature of 220°C and the membranes treated at 230°C but for half the HPT time were similar. For instance, the differences of $\overline{\lambda_w}$, $\overline{d_f}$, ε and θ_w between the ENMs 5 and 9 (220°C/120 min and 230°C/60 min) were smaller than 2.7% while for the ENMs 6 and 10 (220°C/180 min and 230°C/90 min) the differences were smaller than 4.8%. Therefore, similar filtration properties (i.e. selectivity and permeation fluxes) of these membranes are expected.

3.3. MF tests

As mentioned above, electrospun nanofibers exhibit, due to their nanostructure, very large water contact angles compared to polymeric films made from the same material (i.e. phase inversion flat membrane prepared with the same polymer). In this study, PSU ENMs exhibited contact angles between 115-137°. However, phase-inversion PSU membranes are reported to exhibit contact angle values around 70–80° [7]. Therefore, there is an initial 'resistance' for water to enter a completely dry ENM. Once the ENM is wetted, the high void volume fraction of the ENM leads to relatively high flow rates. ENMs are prone to be compressed during filtration because of their high void volume fraction and their relatively poor nanofiber adhesion. Therefore, to open and wet all the inter-fiber spaces of the PSU ENMs and to ensure that the water permeate flux kept constant with filtration time at an applied pressure, a water compaction step was carried out before the MF tests. Subsequently, HA MF tests were conducted with a 15 mg/L HA solution at pH 11 for all the PSU ENMs. The filtration results of all the PSU ENMs are summarized in Table 2.

3.3.1. Effects of the HPT temperature and time on the filtration performance of PSU ENMs

The effects of the HPT temperature and time on the filtration performance of the PSU ENMs were evaluated analysing the changes of the HA permeate fluxes (J_{HA}), the HA separation factor (α) and the irreversible fouling factors (FR_W) (Figs. 6A and B, shown as an example) with the filtration time, and by comparing their performance indexes (PI) (Fig. 8).

Fig. 6A shows the effects of increasing the HPT temperature (at a fixed HPT time of 90 min) from 210°C to 230°C (PSU EMNs 2, 4, and 11). A considerable decrease of J_{HA} along with a gradual increase of α and FR_W was observed. The final HA permeate flux

(J_{HA_f}) of the PSU ENMs decreased by 82.2% when increasing the HPT temperature from 210 to 220°C (ENM 2 to ENM 4) and by 70.6%, when increasing the HPT temperature from 220 to 230°C (ENM 4 to ENM 11). The final HA separation factor (α_f) of ENM 4 (220°C) was 88.9% larger than that of ENM 2 (220°C) and that of ENM 11 (230°C) was 55.9% larger than that of ENM 4. However, the respective changes of FR_W (3.6 and 2.7%) were not as noticeable as those of J_{HA} and α.

The initial permeate flux decline (FD_0) was 0.15, 0.19 and 0.92 for ENM 2, ENM 4 and ENM 11, respectively. This means that the permeate flux of the membrane prepared with the lowest HPT temperature (210°C, ENM 2) was reduced only by 15% during the first minutes of HA filtration whereas that of the membrane prepared with a higher HPT temperature (230°C, ENM 11) was declined by 92%.

These differences in the filtration performance of the membranes are mainly related to their different structural morphology. For instance, the membrane prepared with low HPT temperature (210°C, ENM 2) exhibited the largest $\overline{d_f}$ (3.1 μm) and ε (92.8%) and, therefore had the highest mean HA permeate flux (i.e. average of all the HA permeate fluxes during the MF test; $\overline{J_{HA}}$ = 8406 kg/m^2.h) with the lowest α_f value (3.7%). On the other hand, the membrane treated with the highest temperature (230°C, ENM 11) had the smallest $\overline{d_f}$ (2.6 μm) and ε (78.2%) values and exhibited the lowest $\overline{J_{HA}}$ (358 kg/m^2.h) with the highest α_f (75%) values. It is worth nothing that although the ENM 11 had a $\overline{J_{HA}}$ value of 92.3% lower than that of ENM 2, its *PI* value resulted to be higher (74 kg/m^2.h) than that of the ENM 2 (70 kg/m^2.h) because of its larger separation factor. Similar results were reported by Li et al. [26] with poly (lactic acid) (PLA) ENMs when increasing the HPT temperature from 90 to 95°C (at a fixed HPT time of 30 min). A decrease in the inter-fiber space of these membranes (from 2.3 to 2.0 μm) resulted in a permeate flux

485 decline (from about 26000 to 8500 L/m^{2}h) along with an increase of the separation factor
486 of TiO_2 particles (from 61 to 85%).

487 Fig. 6B shows the effects of the HPT time (at a fixed HPT temperature of 230°C) on
488 the filtration performance of the PSU EMNs 8 (45 min), 9 (60 min), 10 (75 min) and 11
489 (90 min). In this case, the effects on J_{HA} and α when increasing the HPT time from 45 to
490 90 min were not as noticeable as those observed when the HPT temperature was increased
491 from 210 to 230°C. For instance, a gradual reduction of J_{HA_f} (20.9, 22.3 and 47.3%) and
492 an increase of α_f (41.8, 10.3 and 5.6%) were observed when increasing the HPT time
493 from 45 to 60, from 60 to 75 and from 75 to 90 min, respectively. The FR_W values did not
494 follow a clear trend. The membrane with the lowest value of FR_W (95.9%) was the one
495 treated for 60 min (ENM 6).

496 The values of FD_0 for the ENMs 8, 9, 10 and 11 were 0.40, 0.55, 0.79 and 0.92,
497 respectively, indicating that the initial permeate flux decline increased progressively
498 when increasing the HPT time. It can also be noticed in Fig. 6B that all membranes
499 reached a relatively constant J_{HA} value after 360 min of filtration time. As mentioned
500 before, the changes in filtration performance of the PSU ENMs are directly related to
501 their morphological and structural changes. The longer the HPT treatment time, the more
502 compacted was the membrane structure and the thicker and more interconnected were
503 their nanofibers (i.e. higher $\overline{\lambda_w}$ and smaller $\overline{d_f}$; see Table 1, Fig. 3, and Fig. 5B). These
504 resulted in a reduction of $\overline{J_{HA}}$ from 3481 kg/m^2 for ENM 8 (45 min) to 358 kg/m^2.h for
505 ENM 11 (90 min) and an enhancement of α_f from 37.0 to 75.0%, respectively (see Table
506 2). The membranes prepared with the lowest HPT time (ENM 8, 113 kg/m^2.h) and the
507 highest HPT time (ENM 11, 74 kg/m^2.h) both had smaller *PI* values than those treated
508 for intermediate HPT times (ENM 9, 147 kg/m^2.h, and ENM 10, 133 kg/m^2.h).

As mentioned in the introduction, fouling is a major factor limiting the application of membranes in water treatment. Thus, a characterization analysis of the organic fouling generated on the membranes after MF tests was conducted. FTIR, SEM imaging and EDS mapping were used to confirm the presence of HA across the PSU ENMs, to compare the surface morphology of the membranes before and after filtration and to measure the change of the atomic composition of the membranes due to the organic fouling (Fig. S5).

The J_{HA} and α curves plotted in Fig. 6 can be used to study the fouling phenomenon of the PSU ENMs. HA fouling in MF membranes has two stages: i) a pore blockage that corresponds to a rapid HA permeate flux decline due to the deposition of large HA aggregates on the surface and in the pores (inter-fiber space for ENMs) of the membrane as well; ii) a cake filtration that induces a slow decrease of the HA permeate flux with filtration time until a relatively constant value of the permeate flux (known as steady-state value or asymptotic permeate flux) is reached. During this second stage a HA deposit or cake layer forms on those regions of the membrane that were covered by HA aggregates during the first stage [14, 41-44].

The transition between the pore blockage and the cake filtration stage is usually determined by the change of the slopes of both the permeate flux and separation factor curves with filtration time. The time (t_c) at which this change occurs is known as the "critical point". A smaller t_c indicates a shorter length of the initial pore blocking stage, and hence a faster fouling evolution rate. The value of t_c depends mainly on the morphological and structural characteristics of each PSU ENM (e.g. mean size of the inter-fiber space, inter-fiber space distribution, void volume fraction, mean nanofiber diameter, hydrophobicity, etc.).

From Fig. 6B it can be seen that the pore blockage of the PSU ENMs prepared with higher HPTs (i.e. ENMs 9, 10 and 11) occurred faster, during the first half an hour of filtration (t_c < 30 min). This is attributed to their more compact structure and smaller size of the inter-fiber space, which promotes the pore blockage phenomenon [45, 46]. For these membranes, the slope of the α curve was relatively small until the critical time t_c (i.e. beginning of pore blockage stage) was reached. Subsequently, a considerable increase of α was observed (due to the reduction of the membrane inter-fiber space during the pore blockage stage and during the formation and growth of the cake layer in the second stage), followed by a slower increase of α (attributed to the reached cake layer mature stage). A relatively steady-state value of the HA separation factor (α_f) was obtained at the end of the filtration test (70.9, 75.0 and 77.6% for the ENMs 9, 10 and 11, respectively).

For the membranes prepared with low HPTs (i.e. ENMs 4 and 8, see Figs. 6A and B), the slope of the α curve was relatively constant and close to zero during the first 125 minutes of filtration (i.e. pore blockage stage with $t_c \approx 125$ min). Then it increased considerably during the next 300 min of filtration time (i.e. cake filtration), reaching values up to 37%. The membrane prepared with the lowest HPT (i.e. ENM 2) did not retain HA, most likely due to the low quantity of bonding points between nanofibers (see SEM image in Fig 2). Unbounded nanofibers may be displaced by the hydrostatic water pressure leading to a broad inter-fiber space of the ENM and allowing HA particles to penetrate through the membrane resulting in no separation. The α_f values of all the PSU ENMs ranged from 1 to 78% (see Table 2). This elucidates the clear differences of the morphological characteristics of the PSU ENMs and confirms the important influence of the HPT on the filtration performance of the membranes.

In the previous section it was reported that the morphological and structural characteristics of the membranes treated at a HPT temperature of 220°C during a time *t* and those treated at 230°C during a time t/2 were very similar. For this reason, a comparison of the filtration properties (i.e. J_{HA}, α and FR_W) of the membrane pairs ENMs 4-8, 5-9, 6-10 and 7-11 was performed (Fig. 7). Their J_{HA_f} values were approximately the same (see Table 2) with deviations below 10.2%. Similarly, the same tendency was observed for the curves of α as a function of filtration time for each pair of membranes. In particular, the α curves of the membranes prepared with lower HPTs (i.e. ENMs 4 and 8) overlapped, while only small differences were detected for the pairs of membranes prepared with higher HPTs (i.e. ENMs 5-9, 6-10 and 7-11). Taking into account their mean α for the entire filtration process ($\bar{\alpha}$), the deviation between these values was low and ranged between 4.1 and 11.9%, the maximum deviation corresponding to the membranes prepared with the highest HPTs (i.e. EMN 7 ($\bar{\alpha} = 39.6\%$) and ENM 11 ($\bar{\alpha} = 45.0\%$)). It is worth noting that despite the similarities in the filtration behaviour of the pairs of membranes, higher α_f values were obtained for all the membranes treated at 230°C compared to those treated at 220°C for a double HPT time. By comparing the values of FR_W of the different pairs of membranes (Table 2 and Fig. 7) no clear conclusion could be drawn. The deviation of the FR_W values of the pairs of membranes prepared with higher HPTs (i.e. ENMs 6-10 and 7-11) was smaller than 0.2%, while the highest deviation (2.5%) was reached for the pair of ENMs 5-9.

Despite the similarities in the filtration characteristics between the pairs of membranes, PSU ENMs treated at 230°C had up to 16.4% greater *PI* values than PSU ENMs treated at 220°C. Therefore, it is advisable to increase the HPT temperature by 10°C and reduce the HPT time by half as it permits energy and cost savings.

3.3.2. Comparative study

The pure water permeability (*PWP*) of all prepared PSU ENMs measured after compaction ranged from 15260 to 20563 kg/m^2.h.bar, which is 3-fold to 100-fold higher than those achieved by highly porous lab-made PSU ENMs (1472-5648 kg/m^2.h.bar) [3] and PVDF ENMs (232-1984 kg/m^2.h.bar) [2] used for particulate removal, and similar or greater than those reported for mechanically enhanced lab-made PES ENMs (16006 kg/m^2.h.bar) [47]. In addition, the *PWP* values obtained in the present study for PSU ENMs were larger than those of commercial flat sheet membranes typically used in MF processes (i.e. PVDF MF: 2436 kg/m^2.h.bar, Model V0.2, Synder Membrane Technology [47]; PES tight MF: 327 kg/m^2.h.bar, Model LX, Synder Membrane Technology [47]; GVHP MF: 8875 kg/m^2.h.bar, Millipore [43]; PES OMEGA MF: 6783 kg/m^2.h.bar, Filtron Technology [12]; PVDF DURAPORE MF: 5217 kg/m^2.h.bar, Millipore [12]; PES HPWP MF: 14761 kg/m^2.h.bar, Millipore; see Table 3). These values confirm the structural advantages of the ENMs over traditional water filtration membranes, such as their three-dimensional-inter-pore connectivity and high void volume fractions (i.e. higher porosity leads to more channels for water flow) [46, 48]. In addition, the treated PSU ENMs had a small water entry pressure (below 1 bar), which is convenient for low-pressure water purification and therefore for MF applications.

(**Table 3**: Ref. [2, 3, 7, 12, 26, 43, 47, 49])

In this study, the final permeate fluxes (J_f) measured after 7 hours of filtration for the PSU ENMs with the highest *PI* values (i.e. ENMs 9 and 10) are 188 and 232 kg/m^2.h (Table 3). These values are 3.7 to 4.5 times greater than the obtained one in our previous study (51.3 kg/m^2.h) [7]. In addition, the values of α_f of ENMs 9 and 10 are 6.5 and 18.2%

603 greater than the highest value obtained in our former work (60%) [7]. Thus, the optimized
604 HPT improved the filtration performance index (*PI*) of the membranes up to 5-fold [7].

605 The final normalized permeate fluxes (J_f) by the applied pressure (ΔP) of the ENMs 9
606 and 10 (232 and 188 kg/m^2.h.bar) are 63 and 32% greater than that of the eco-efficient,
607 micro-porous, lab-made PLA ENM 1 (143 kg/m^2.h.bar) [26]. The values of α_f measured
608 for ENMs 9 and 10 are also 5 and 16% higher than that of the PLA ENM 1. The values
609 of *PI* of ENMs 9 and 10 are therefore 53 and 69% greater than that of PLA ENM 1, which
610 confirms the high filtration performance of the heat-treated optimized ENMs.

611 The commercial MF membranes (PES MF, PVDF MF and PCTE MF) used by Yuan
612 and Zydney [12] for the treatment of 2 mg/L HA solutions had up to 33% smaller J_f
613 values than those of the PSU ENMs 9 and 10, which were used to treat higher
614 concentrated HA solutions (15 mg/L). This is probably due to their lower porosity and
615 smaller mean pore size. However, the commercial MF membranes exhibited higher α_f
616 values (up to 49%) when compared with the PSU ENMs 9 and 10, mainly caused by their
617 smaller mean pore size. Considering that the average size of HA particles in a basic
618 environment ranges from 0.3 to 4 nm [7] and the mean size of the inter-fiber space of the
619 PSU ENMs ranges from 2 to 4 μm, the values of α_f obtained for the ENMs 9 and 10 (63.9
620 and 70.9%, respectively) can be considered reasonably good. The measured values of α_f
621 are probably affected by both the high tortuosity of the ENMs (i.e. HA molecules are
622 expected to be more prone to mechanical entrapment in the thread-like network of an
623 ENM [46]) and the rejection mechanism in a fibrous structured membrane, which
624 includes sieving, electrostatic attraction, diffusion and inertia [47].

625 For sake of comparison, a commercial PES MF membrane (HPWP, hydrophilic,
626 Millipore) was tested in this study following exactly the same filtration procedure than

627 that of the PSU ENMs. The results are also summarized in Table 3. The PES MF
628 commercial membrane has lower J_f value (up to 55%) but a higher α_f (up to 18%) than
629 the ENMs 9 and 10. However, its *PI* value (82 kg/m^2.h) is 44 and 38% lower than that of
630 the ENMs 9 and 10 (i.e. 147 and 133 kg/m^2.h, respectively) (Fig. S6 in SI). This result
631 elucidates the good performance of the treated-optimized PSU ENMs for MF
632 applications.

633 The values of FR_W obtained for all PSU ENMs ranged from 81.9 to 99%, and are higher
634 than those reported by Schäfer et al. [43] during MF of 20 mg/L HA solution at pH 8
635 (81%) and 5 mg/L HA solution at pH 10 (73%) with a MF commercial hydrophilic
636 membrane (GVWP, 0.22 μm pore size; Millipore). The reduction of the irreversible
637 fouling factor of PSU ENMs is important to extend the membrane lifetime for filtration
638 application. Different ways have been adopted to improve the FR_W including surface
639 modification of ENMs by interfacial polymerization (IP) technique [33, 50].

640 Compared to other ENMs with HPT used for filtration [2, 5, 7, 24, 26, 37, 51, 52], the
641 total manufacturing time of PSU ENMs of the present study was shorter. For other
642 reported membranes the electrospinning process took between 1 and 8 hours, up to 10
643 times longer than the electrospinning fabrication time (t_e) used in this study (45 min). In
644 addition, the HPT times used for the treated-optimized PSU ENMs of the present study
645 were 60-75 min, up to 18-fold shorter than the time (120-1080 min) reported for other
646 membranes.
647

648 **4. Conclusions**

649 Different HPTs were investigated to improve the filtration performance of PSU
650 ENMs. The effects of the HPT temperature (i.e. 210, 220, 230°C) and time (i.e. 45, 60,

75, 90, 120, 150, 180 min) on their morphology and structure were studied systematically. It was observed that increasing either the HPT temperature or time resulted in a reduction of $\overline{d_f}$ along with an increase of both $\overline{\lambda_w}$ and the number of connections between nanofibers, which led to an improvement of the structural integrity of the membranes. A gradual decrease of the ε and θ_w values of the PSU ENMs was obtained when the HPT temperature or the HPT time was increased, which resulted in membranes with smoother surfaces. No connection points between nanofibers could be detected when the membranes were prepared at a low HPT temperature (ENMs 1-2 (210°C)) or for a short HPT time (ENMs 3 (60 min) and 8 (45 min)).

The main effects of increasing either the HPT temperature or the HPT time on the filtration properties of the membranes were a reduction of the HA permeate flux and an improvement of the HA separation factor.

It was observed that the fouling evolution rate of the PSU ENMs prepared with higher HPTs (i.e. ENMs 10 and 11) was faster. Pore blockage occurred earlier (t_c < 30 min) in these membranes compared to those prepared with lower HPTs (i.e. ENMs 4 and 8), in which pore blockage took place during the first 125 minutes of the filtration process.

Similar morphological characteristics as well as filtration performance were observed for the membranes treated at 220°C and those treated at 230°C for half the heating time. Despite these similarities, the values of α_f of the membranes treated at 230°C were up to 14.6% higher than those of the membranes treated at 220°C, resulting in up to 16.4% better performance indexes. From these results it can be concluded that it is better to perform HPT at a higher temperature, because the reduction in HPT time permits energy and cost savings.

Compared to the best PSU ENMs (i.e. ENMs 9 and 10), lower *PI* value was obtained for the commercial PES MF membrane (HPWP, Millipore) tested under the same

filtration procedure to that followed for the PSU ENMs. This confirms the good performance of the prepared PSU ENMs for MF applications.

The significantly higher *PWP* of PSU ENMs compared to commercial flat sheet filtration membranes allows the use of lower pressures and thus reduces energy consumption during filtration. Together with their short manufacturing time, this property makes PSU ENMs fabricated with the optimized HPT conditions very promising candidates to reduce the overall costs and energy consumption of MF applications.

Acknowledgments

The authors gratefully acknowledge the financial support of the Spanish Ministry of Economy and Competitiveness through its project CTM2015-65348-C2-2-R. P. Arribas is thankful to the Campus of International Excellence, Moncloa Campus (UCM-UPM), for the PhD grant.

References

[1] Y. Huang, Q.L. Huang, H. Liu, C.X. Zhang, Y.W. You, N.N. Li, C.F. Xiao, Preparation, characterization, and applications of electrospun ultrafine fibrous PTFE porous membranes, J. Membr. Sci., 523 (2017) 317-326.
[2] R. Gopal, S. Kaur, Z. Ma, C. Chan, S. Ramakrishna, T. Matsuura, Electrospun nanofibrous filtration membrane, J. Membr. Sci., 281 (2006) 581-586.
[3] R. Gopal, S. Kaur, C.Y. Feng, C. Chan, S. Ramakrishna, S. Tabe, T. Matsuura, Electrospun nanofibrous polysulfone membranes as pre-filters: Particulate removal, J. Membr. Sci., 289 (2007) 210-219.
[4] J. Doshi, D.H. Reneker, Electrospinning process and applications of electrospun fibers, J. Electrostat., 35 (1995) 151-160.
[5] Z. Ma, M. Kotaki, S. Ramakrishna, Surface modified nonwoven polysulphone (PSU) fiber mesh by electrospinning: A novel affinity membrane, J. Membr. Sci., 272 (2006) 179-187.
[6] S.-S. Choi, Y.S. Lee, C.W. Joo, S.G. Lee, J.K. Park, K.-S. Han, Electrospun PVDF nanofiber web as polymer electrolyte or separator, Electrochim. Acta, 50 (2004) 339-343.
[7] P. Arribas, M. Khayet, M.C. García-Payo, L. Gil, Self-sustained electro-spun polysulfone nano-fibrous membranes and their surface modification by interfacial polymerization for micro- and ultra-filtration, Sep. Purif. Technol., 138 (2014) 118-129.
[8] Y. Liu, R. Wang, H. Ma, B.S. Hsiao, B. Chu, High-flux microfiltration filters based on electrospun polyvinylalcohol nanofibrous membranes, Polymer, 54 (2013) 548-556.

709 [9] S. Homaeigohar, J. Koll, E.T. Lilleodden, M. Elbahri, The solvent induced interfiber adhesion
710 and its influence on the mechanical and filtration properties of polyethersulfone electrospun
711 nanofibrous microfiltration membranes, Sep. Purif. Technol., 98 (2012) 456-463.
712 [10] H.-C. Kim, B.G. Choi, J. Noh, K.G. Song, S.-h. Lee, S.K. Maeng, Electrospun nanofibrous PVDF–
713 PMMA MF membrane in laboratory and pilot-scale study treating wastewater from Seoul Zoo,
714 Desalination, 346 (2014) 107-114.
715 [11] A. Baji, Y.-W. Mai, S.-C. Wong, M. Abtahi, P. Chen, Electrospinning of polymer nanofibers:
716 Effects on oriented morphology, structures and tensile properties, Compos. Sci. Technol., 70
717 (2010) 703-718.
718 [12] W. Yuan, A.L. Zydney, Humic acid fouling during microfiltration, J. Membr. Sci., 157 (1999)
719 1-12.
720 [13] N. Yang, X. Wen, T.D. Waite, X. Wang, X. Huang, Natural organic matter fouling of
721 microfiltration membranes: Prediction of constant flux behavior from constant pressure
722 materials properties determination, J. Membr. Sci., 366 (2011) 192-202.
723 [14] R. Seifollahy Astaraee, T. Mohammadi, N. Kasiri, Analysis of BSA, dextran and humic acid
724 fouling during microfiltration, experimental and modeling, Food Bioprod. Process., 94 (2015)
725 331-341.
726 [15] Y. Su, C. Li, W. Zhao, Q. Shi, H. Wang, Z. Jiang, S. Zhu, Modification of polyethersulfone
727 ultrafiltration membranes with phosphorylcholine copolymer can remarkably improve the
728 antifouling and permeation properties, J. Membr. Sci., 322 (2008) 171-177.
729 [16] A.-R. Cho, D.M. Shin, H.W. Jung, J.C. Hyun, J.S. Lee, D. Cho, Y.L. Joo, Effect of annealing on
730 the crystallization and properties of electrospun polylatic acid and nylon 6 fibers, J. Appl. Polym.
731 Sci., 120 (2011) 752-758.
732 [17] L. Huang, S.S. Manickam, J.R. McCutcheon, Increasing strength of electrospun nanofiber
733 membranes for water filtration using solvent vapor, J. Membr. Sci., 436 (2013) 213-220.
734 [18] X. Ran, Z. Jia, C. Han, Y. Yang, L. Dong, Thermal and mechanical properties of blends of
735 polylactide and poly(ethylene glycol-co-propylene glycol): Influence of annealing, J. Appl. Polym.
736 Sci., 116 (2010) 2050-2057.
737 [19] H.-C. Chen, C.-H. Tsai, M.-C. Yang, Mechanical properties and biocompatibility of
738 electrospun polylactide/poly(vinylidene fluoride) mats, J. Polym. Res., 18 (2011) 319-327.
739 [20] S. Kaur, R. Barhate, S. Sundarrajan, T. Matsuura, S. Ramakrishna, Hot pressing of electrospun
740 membrane composite and its influence on separation performance on thin film composite
741 nanofiltration membrane, Desalination, 279 (2011) 201-209.
742 [21] B.S. Lalia, E. Guillen-Burrieza, H.A. Arafat, R. Hashaikeh, Fabrication and characterization of
743 polyvinylidenefluoride-co-hexafluoropropylene (PVDF-HFP) electrospun membranes for direct
744 contact membrane distillation, J. Membr. Sci., 428 (2013) 104-115.
745 [22] Y. Liao, R. Wang, M. Tian, C. Qiu, A.G. Fane, Fabrication of polyvinylidene fluoride (PVDF)
746 nanofiber membranes by electro-spinning for direct contact membrane distillation, J. Membr.
747 Sci., 425-426 (2013) 30-39.
748 [23] Y. You, S. Won Lee, S. Jin Lee, W.H. Park, Thermal interfiber bonding of electrospun poly(l-
749 lactic acid) nanofibers, Mater. Lett., 60 (2006) 1331-1333.
750 [24] S.S. Homaeigohar, K. Buhr, K. Ebert, Polyethersulfone electrospun nanofibrous composite
751 membrane for liquid filtration, J. Membr. Sci., 365 (2010) 68-77.
752 [25] Y. Liang, S. Cheng, J. Zhao, C. Zhang, S. Sun, N. Zhou, Y. Qiu, X. Zhang, Heat treatment of
753 electrospun Polyvinylidene fluoride fibrous membrane separators for rechargeable lithium-ion
754 batteries, J. Power Sources, 240 (2013) 204-211.
755 [26] L. Li, R. Hashaikeh, H.A. Arafat, Development of eco-efficient micro-porous membranes via
756 electrospinning and annealing of poly (lactic acid), J. Membr. Sci., 436 (2013) 57-67.
757 [27] S.S. Homaeigohar, H. Mahdavi, M. Elbahri, Extraordinarily water permeable sol–gel formed
758 nanocomposite nanofibrous membranes, J. Colloid Interface Sci., 366 (2012) 51-56.
759 [28] S.S. Homaeigohar, M. Elbahri, Novel compaction resistant and ductile nanocomposite
760 nanofibrous microfiltration membranes, J. Colloid Interface Sci., 372 (2012) 6-15.

761 [29] Y. Liao, C.H. Loh, M. Tian, R. Wang, A.G. Fane, Progress in electrospun polymeric nanofibrous
762 membranes for water treatment: Fabrication, modification and applications, Prog. Polym. Sci.,
763 77 (2018) 69-94.
764 [30] C. Migliaresi, D. Cohn, A. De Lollis, L. Fambri, Dynamic mechanical and calorimetric analysis
765 of compression-molded PLLA of different molecular weights: Effect of thermal treatments, J.
766 Appl. Polym. Sci., 43 (1991) 83-95.
767 [31] D. Aussawasathien, C. Teerawattananon, A. Vongachariya, Separation of micron to sub-
768 micron particles from water: Electrospun nylon-6 nanofibrous membranes as pre-filters, J.
769 Membr. Sci., 315 (2008) 11-19.
770 [32] K. Smolders, A.C.M. Franken, Terminology for Membrane Distillation, Desalination, 72
771 (1989) 249-262.
772 [33] M.N.A. Seman, M. Khayet, N. Hilal, Nanofiltration thin-film composite polyester
773 polyethersulfone-based membranes prepared by interfacial polymerization, J. Membr. Sci., 348
774 (2010) 109-116.
775 [34] X. Yuan, Y. Zhang, C. Dong, J. Sheng, Morphology of ultrafine polysulfone fibers prepared by
776 electrospinning, Polym. Int., 53 (2004) 1704-1710.
777 [35] L. Liu, Z. Pan, Properties of hydrophilic chitosan/polysulfone nanofibrous filtration
778 membrane, J. Eng. Fiber. Fabr., 9 (2014) 76-86.
779 [36] D. Hussain, F. Loyal, A. Greiner, J.H. Wendorff, Structure property correlations for
780 electrospun nanofiber nonwovens, Polymer, 51 (2010) 3989-3997.
781 [37] M. Essalhi, M. Khayet, Self-sustained webs of polyvinylidene fluoride electrospun
782 nanofibers at different electrospinning times: 1. Desalination by direct contact membrane
783 distillation, J. Membr. Sci., 433 (2013) 167-179.
784 [38] A. Marmur, Wetting on hydrophobic rough surfaces: to be heterogeneous or not to be?,
785 Langmuir, 19 (2003) 8343-8348.
786 [39] B. Bhushan, Y. Chae Jung, Wetting study of patterned surfaces for superhydrophobicity,
787 Ultramicroscopy, 107 (2007) 1033-1041.
788 [40] H. Savoji, D. Rana, T. Matsuura, S. Tabe, C. Feng, Development of plasma and/or chemically
789 induced graft co-polymerized electrospun poly(vinylidene fluoride) membranes for solute
790 separation, Sep. Purif. Technol., 108 (2013) 196-204.
791 [41] S. Hong, M. Elimelech, Chemical and physical aspects of natural organic matter (NOM)
792 fouling of nanofiltration membranes, J. Membr. Sci., 132 (1997) 159-181.
793 [42] C.-C. Ho, A.L. Zydney, A Combined Pore Blockage and Cake Filtration Model for Protein
794 Fouling during Microfiltration, J. Colloid Interface Sci., 232 (2000) 389-399.
795 [43] A.I. Schäfer, U. Schwicker, M.M. Fischer, A.G. Fane, T.D. Waite, Microfiltration of colloids
796 and natural organic matter, J. Membr. Sci., 171 (2000) 151-172.
797 [44] W. Yuan, A. Kocic, A.L. Zydney, Analysis of humic acid fouling during microfiltration using a
798 pore blockage–cake filtration model, J. Membr. Sci., 198 (2002) 51-62.
799 [45] K. Xiao, Y. Shen, X. Huang, An analytical model for membrane fouling evolution associated
800 with gel layer growth during constant pressure stirred dead-end filtration, J. Membr. Sci., 427
801 (2013) 139-149.
802 [46] K. Xiao, J. Sun, Y. Mo, Z. Fang, P. Liang, X. Huang, J. Ma, B. Ma, Effect of membrane pore
803 morphology on microfiltration organic fouling: PTFE/PVDF blend membranes compared with
804 PVDF membranes, Desalination, 343 (2014) 217-225.
805 [47] J. Bae, I. Baek, H. Choi, Mechanically enhanced PES electrospun nanofiber membranes
806 (ENMs) for microfiltration: The effects of ENM properties on membrane performance, Water
807 Res., 105 (2016) 406-412.
808 [48] L. Marbelia, M. Mulier, D. Vandamme, K. Muylaert, A. Szymczyk, I.F.J. Vankelecom,
809 Polyacrylonitrile membranes for microalgae filtration: Influence of porosity, surface charge and
810 microalgae species on membrane fouling, Algal Res., 19 (2016) 128-137.
811 [49] X. Zhuang, L. Shi, K. Jia, B. Cheng, W. Kang, Solution blown nanofibrous membrane for
812 microfiltration, J. Membr. Sci., 429 (2013) 66-70.

[50] M.N. Abu Seman, M. Khayet, N. Hilal, Development of antifouling properties and performance of nanofiltration membranes modified by interfacial polymerisation, Desalination, 273 (2011) 36-47.
[51] A.M. Bazargan, M. Keyanpour-rad, F.A. Hesari, M.E. Ganji, A study on the microfiltration behavior of self-supporting electrospun nanofibrous membrane in water using an optical particle counter, Desalination, 265 (2011) 148-152.
[52] S. Kaur, Z. Ma, R. Gopal, G. Singh, S. Ramakrishna, T. Matsuura, Plasma-Induced Graft Copolymerization of Poly(methacrylic acid) on Electrospun Poly(vinylidene fluoride) Nanofiber Membrane, Langmuir, 23 (2007) 13085-13092.

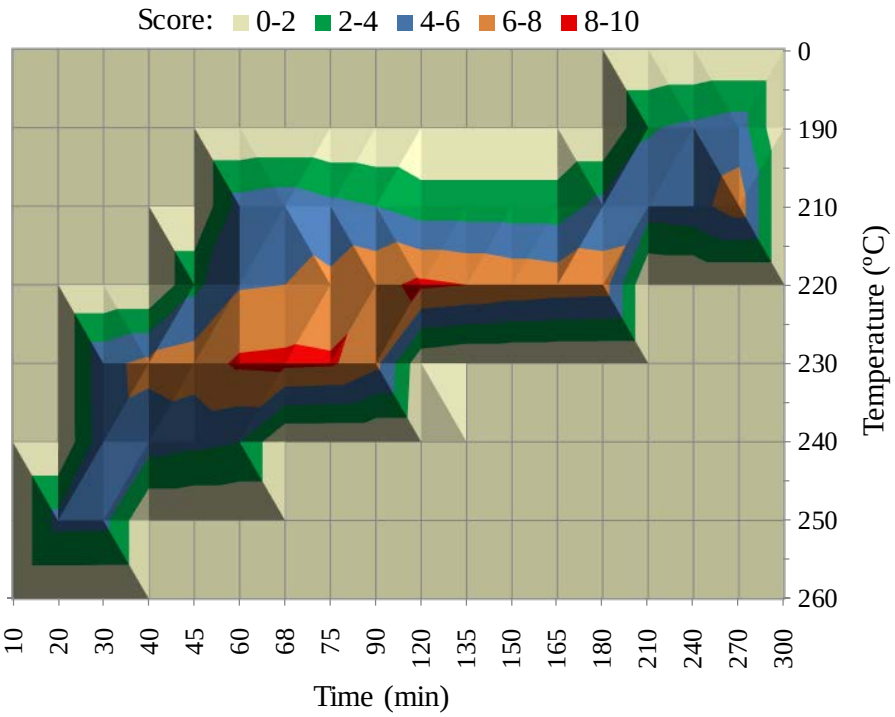

Fig. 1. 3D surface graph showing the result of the preliminary evaluation of the PSU ENMs treated with different heat post-treatments (HPTs).

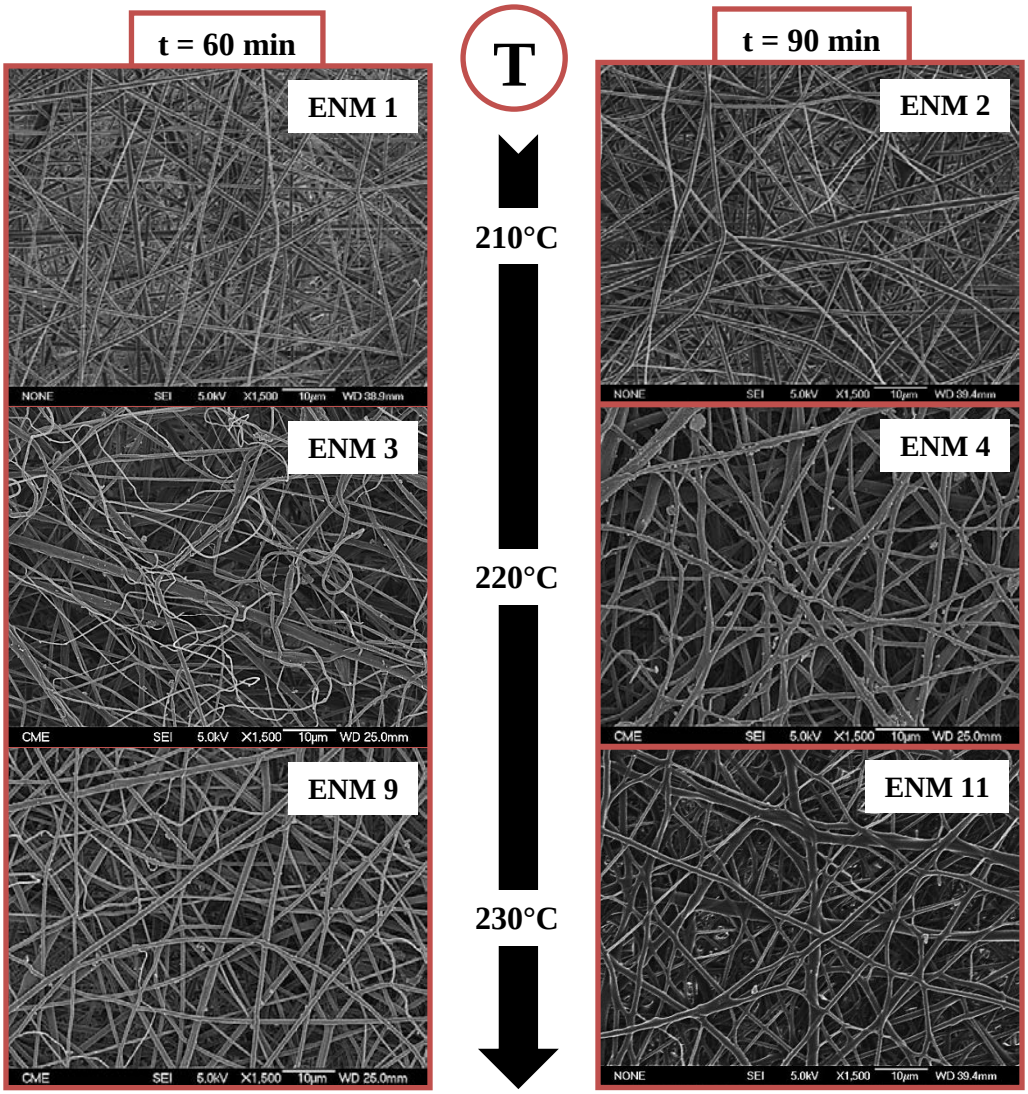

Fig. 2. SEM images of the surface of PSU ENMs prepared with a HPT time of 60 and 90 min at a HPT temperature of 210, 220 and 230°C. All images were taken at X1500 magnification.

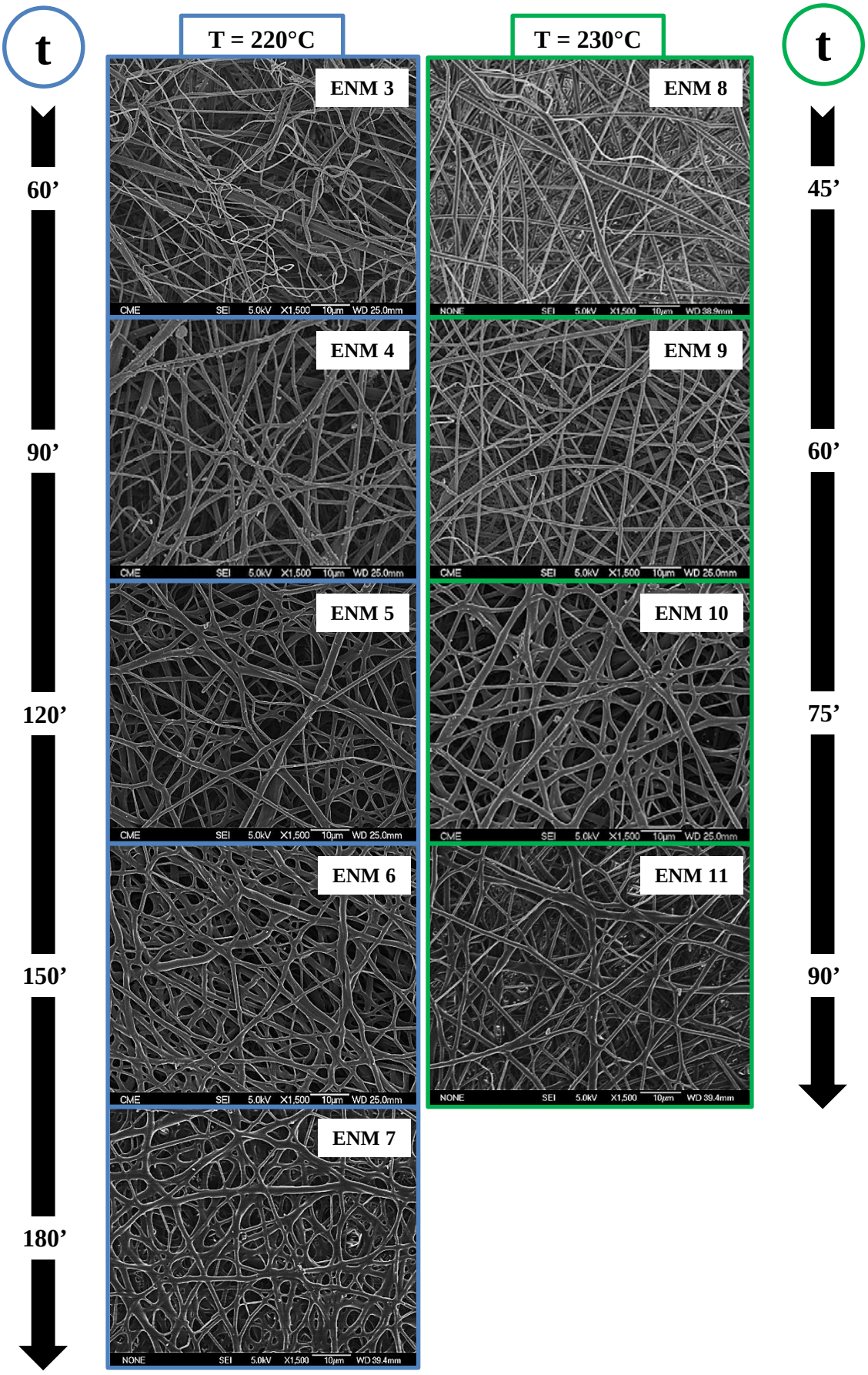

Fig. 3. SEM images of the surface of PSU ENMs prepared with a HPT temperature of 220 and 230°C at different HPT times (from 45 to 180 min). All SEM images were taken at X1500 magnification.

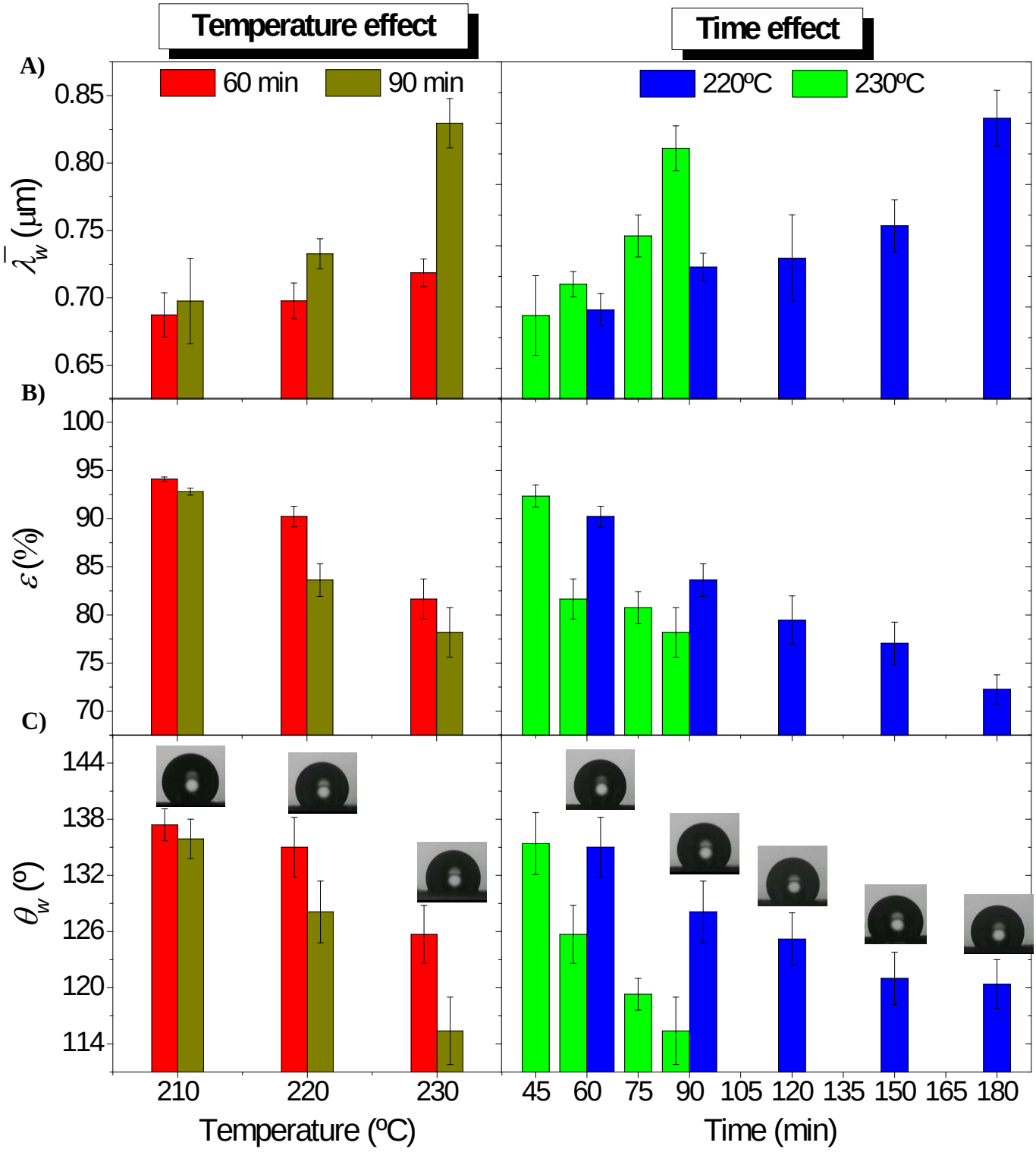

Fig. 4. Effects of HPT temperature and time on the morphological characteristics of PSU ENMs: A) weighted arithmetic mean of the fiber diameters ($\overline{\lambda_w}$), B) void volume fraction (ε) and C) water contact angle (θ_w). Contact angles micrographs in C) are added as supporting information of the graphics.

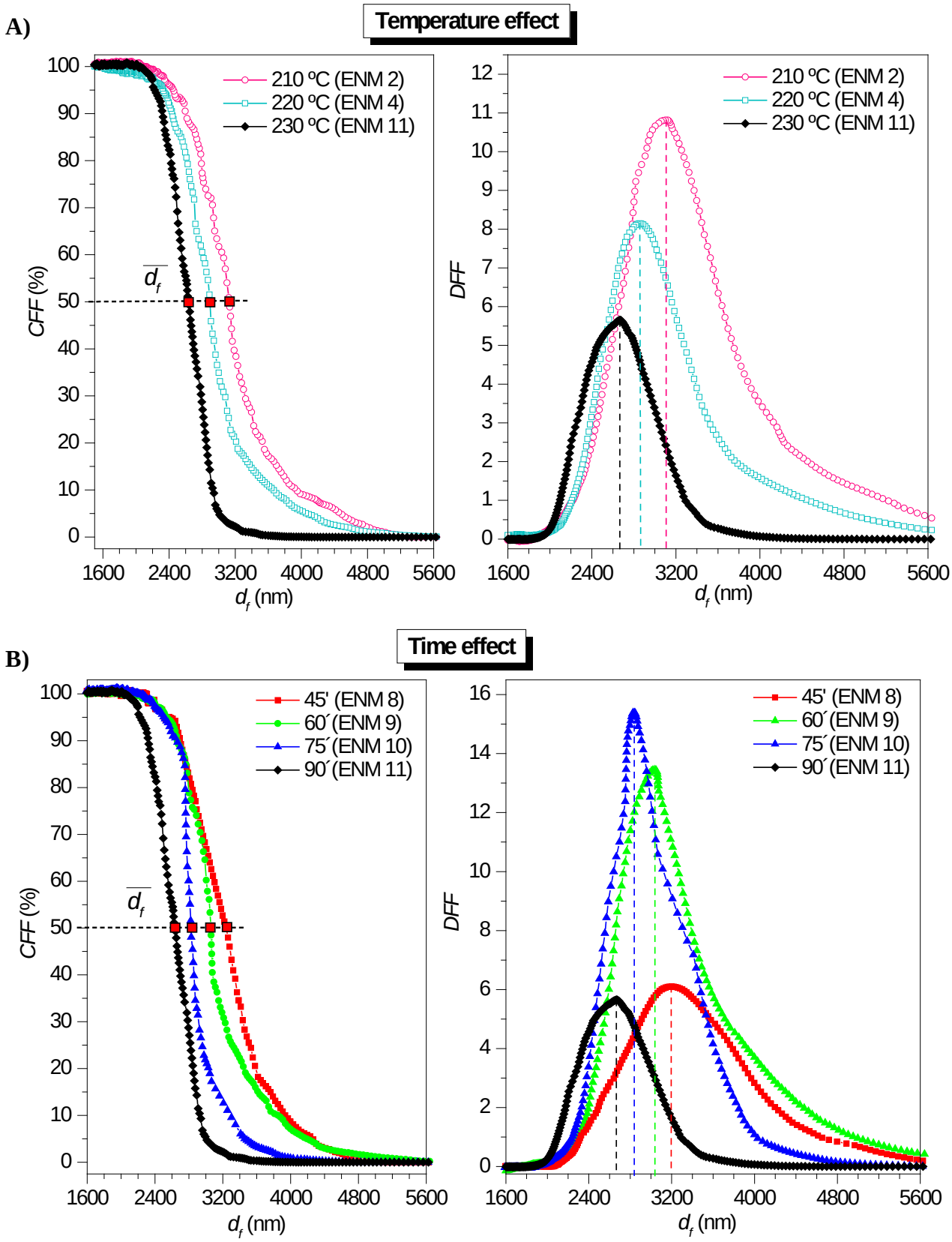

Fig. 5. Effects of HPT temperature (A) and time (B) on the mean size of the inter-fiber space ($\overline{d_f}$), the inter-fiber space distribution or differential filter flow (*DFF*) and the cumulative filter flow distribution (*CFF*) of the PSU ENMs.

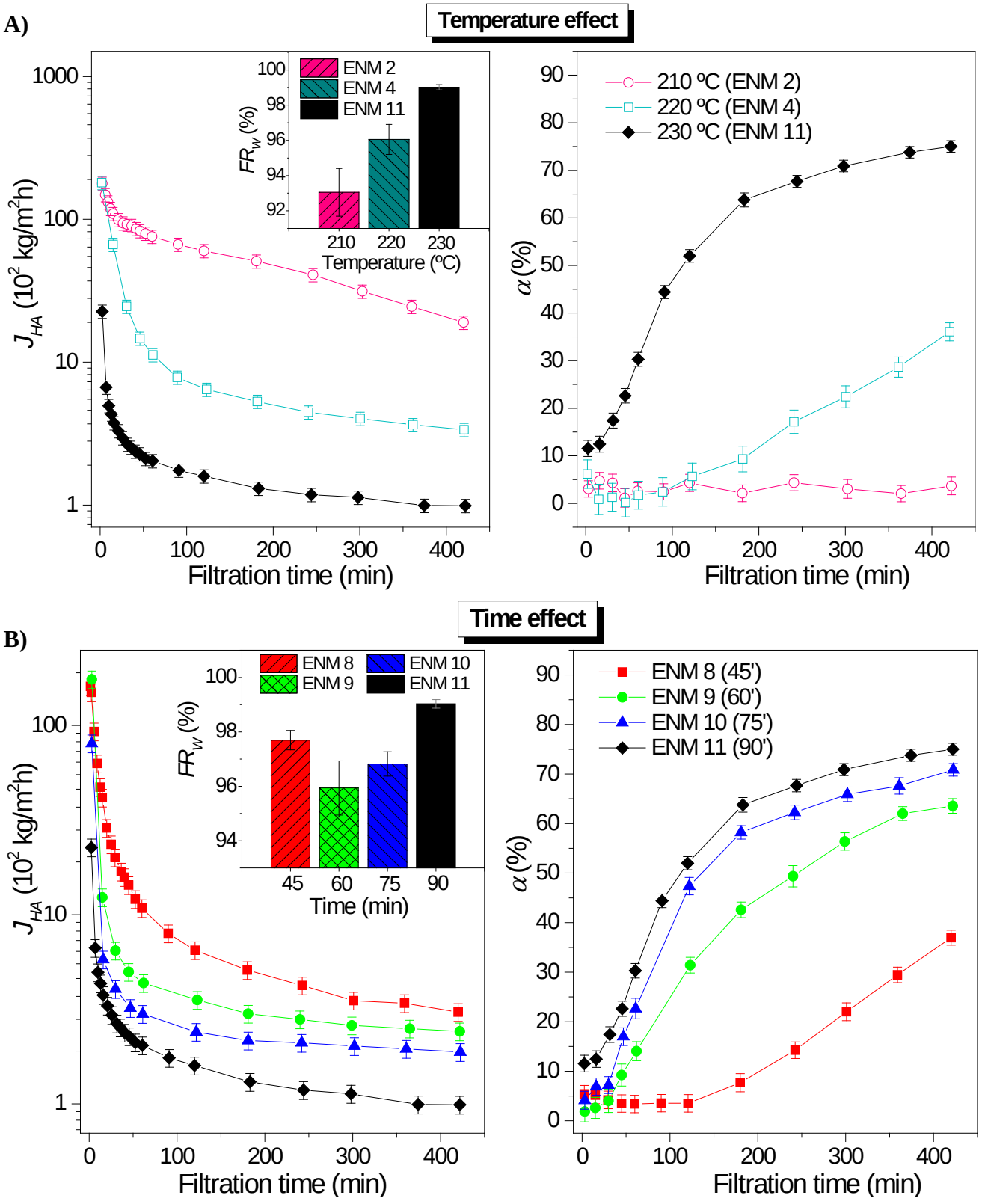

Fig. 6. Humic acid permeate flux (J_{HA}), separation factor (α) and irreversible fouling factor (FR_W) of the PSU ENMs prepared with a HPT temperature of 210, 220 and 230°C for 90 min HPT time (A), and with 230°C HPT temperature for 45, 60, 75 and 90 min HPT time (B). The filtration tests were conducted with 15 mg/L HA feed aqueous solution at pH 11 and 10^5 Pa transmembrane pressure (ΔP).

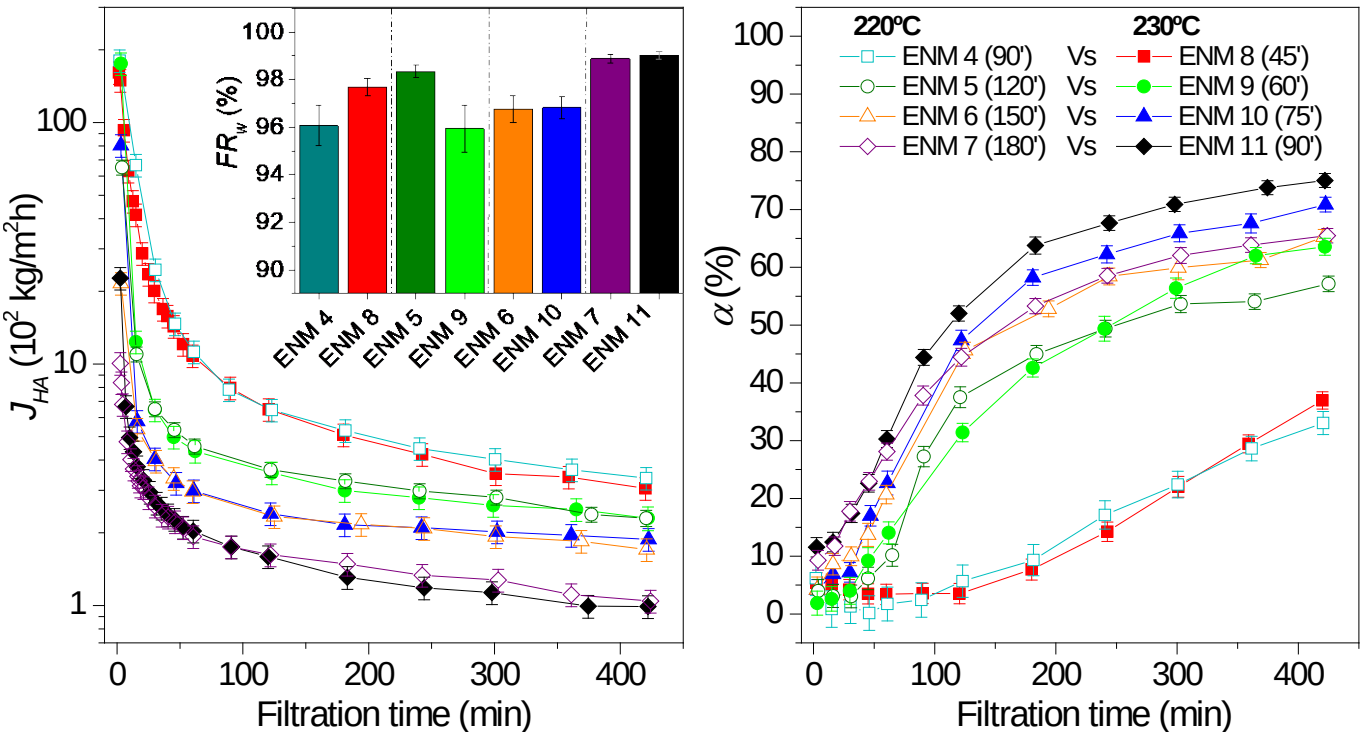

Fig. 7. Humic acid permeate flux (J_{HA}), selectivity (α) and irreversible fouling factor (FR_W) of the PSU ENMs prepared at different HPT conditions. The filtration tests were conducted with 15 mg/L HA feed aqueous solution at pH 11 and 10^5 Pa transmembrane pressure (ΔP).

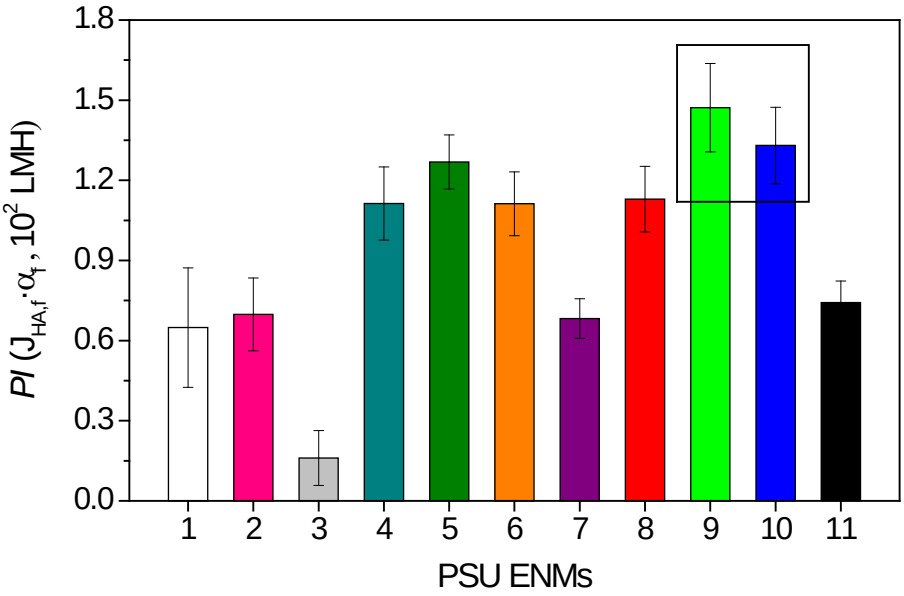

Figure 8: Performance index (*PI*) of the PSU ENMs prepared with different HPT conditions.

Table 1: Prepared PSU ENMs with different heat post-treatments and their corresponding morphological characteristics: thickness (δ), weighted arithmetic mean of the nanofiber diameters ($\overline{\lambda_w}$) with its corresponding weighted standard deviation ($\overline{s_w}$), water contact angle (θ_w), void volume fraction (ε) and mean size of the inter-fiber space ($\overline{d_f}$).

Membrane	Heat treatment		Morphological characteristics				
	T (°C)	t (min)	δ (µm)	$\overline{\lambda_w} \pm \overline{s_w}$ (µm)	θ_w (°)	ε (%)	$\overline{d_f}$ (µm)
ENM 1	210	60	338 ± 15	0.69 ± 0.03	137.4 ± 1.7	94.1 ± 0.2	3.35 ± 0.03
ENM 2	210	90	373 ± 24	0.70 ± 0.06	135.9 ± 2.1	92.8 ± 0.4	3.12 ± 0.02
ENM 3	220	60	380 ± 69	0.70 ± 0.03	135.0 ± 3.2	90.2 ± 1.1	2.98 ± 0.03
ENM 4	220	90	251 ± 47	0.73 ± 0.02	128.1 ± 3.3	83.6 ± 1.7	2.89 ± 0.05
ENM 5	220	120	116 ± 33	0.74 ± 0.07	125.2 ± 2.8	79.5 ± 2.5	2.80 ± 0.05
ENM 6	220	150	106 ± 18	0.77 ± 0.04	121.0 ± 2.8	77.1 ± 2.2	2.72 ± 0.05
ENM 7	220	180	92 ± 18	0.85 ± 0.04	120.4 ± 2.6	72.3 ± 1.5	2.65 ± 0.05
ENM 8	230	45	257 ± 17	0.69 ± 0.06	135.4 ± 3.3	92.3 ± 1.2	3.20 ± 0.04
ENM 9	230	60	213 ± 65	0.72 ± 0.02	125.7 ± 3.1	81.7 ± 2.1	3.04 ± 0.05
ENM 10	230	75	82 ± 29	0.76 ± 0.03	119.3 ± 1.7	80.8 ± 1.7	2.85 ± 0.03
ENM 11	230	90	147 ± 17	0.83 ± 0.04	115.4 ± 3.6	78.2 ± 2.6	2.67 ± 0.03

Table 2: Filtration performance of PSU ENMs prepared with different heat post-treatments: initial water permeate flux (J_{w0}), mean humic acid (HA) permeate flux ($\overline{J_{HA}}$), final HA permeate flux (J_{HAf}), final HA separation factor (α_f), irreversible fouling factor (FR_w) and performance index (PI).

Membrane	Heat treatment		Filtration characteristics					
	T (ºC)	t (min)	J_{w0} $\left(10^2 \frac{kg}{m^2 h}\right)$	$\overline{J_{HA}}$ $\left(10^2 \frac{kg}{m^2 h}\right)$	J_{HAf} $\left(\frac{kg}{m^2 h}\right)$	α_f (%)	FR_w (%)	PI $\left(\frac{kg}{m^2 h}\right)$
ENM 1	210	60	196 ± 21	116 ± 12	8590 ± 919	0.8 ± 1.0	81.9 ± 2.8	65 ± 22
ENM 2	210	90	199 ± 22	84.1 ± 9.0	1899 ± 203	3.7 ± 1.2	93.1 ± 1.1	70 ± 14
ENM 3	220	60	205 ± 22	66.6 ± 7.1	1923 ± 206	0.8 ± 1.1	91.7 ± 1.3	16 ± 10
ENM 4	220	90	204 ± 22	27.7 ± 3.0	337 ± 36	33.1 ± 2.0	96.4 ± 0.5	111 ± 14
ENM 5	220	120	194 ± 19	10.0 ± 0.7	222 ± 18	57.2 ± 0.6	98.3 ± 0.3	127 ± 10
ENM 6	220	150	182 ± 19	4.5 ± 0.5	170 ± 18	65.3 ± 0.5	96.8 ± 0.5	111 ± 12
ENM 7	220	180	153 ± 17	3.2 ± 0.3	104 ± 11	65.5 ± 0.4	98.9 ± 0.2	68 ± 7
ENM 8	230	45	184 ± 20	34.8 ± 3.7	306 ± 33	37.0 ± 0.6	97.7 ± 0.4	113 ± 12
ENM 9	230	60	206 ± 22	20.0 ± 2.1	232 ± 26	63.6 ± 0.7	95.9 ± 0.6	147 ± 17
ENM 10	230	75	203 ± 22	9.9 ± 1.1	188 ± 20	70.9 ± 0.4	96.8 ± 0.5	133 ± 14
ENM 11	230	90	156 ± 17	3.6 ± 0.4	99 ± 11	75.0 ± 0.3	99.0 ± 0.1	74 ± 8

Table 3: Morphological characteristics and filtration performance of lab-made ENMs and commercial MF membranes: thickness (δ), void volume fraction (ε), mean pore size (MPS), mean nanofiber diameter ($\overline{\lambda_f}$), transmembrane pressure (ΔP), pure water permeability (PWP), initial water permeate flux (J_{w0}), initial permeate flux (J_i), final permeate flux (J_f), final water flux (J_{wf}), final separation factor (α_f) and irreversible fouling factor (FR_w).

Membrane[1]	Morphological characteristics				Filtration performance											Ref
	δ (μm)	ε (%)	MPS (μm)	$\overline{\lambda_f}$ (nm)	Filtration mode	ΔP (bar)	PWP[2] (LMH /bar)	Solution[3]	Particle size (μm)	J_{w0} (LMH)	J_i[4] (LMH)	J_f (LMH)	J_{wf} (LMH)	α_f (%)	FR_W (%)	
PSU ENM^L	135	-	2.1	470	Dead-end	0.5	4568	10 ppm PS Ms	1	2284	1000	538	675	92	70	[3]
							4924		0.5	2462	1867	1433	1120	47	55	
							5544		0.1	2772	2667	2438	2684	14	3	
PVDF ENM^L	300	-	4-10.6	360	Dead-end	0.57	351	500 ppm PS Ms	5	200	200	133	200	91	0	[2]
						0.66	1970	100 ppm PS Ms	1	1300	1066	530	530	98	59	
PES ENM^L	200	76.5	0.42	600	Dead-end	1	16006	Kaolin Ms	1.6	16006	15990	3143	11844	100	26	[47]
PES tight MF^C	220	-	0.1	-	Dead-end	1	2436	Kaolin Ms	1.6	2436	2421	1000	-	99.4	-	
PVDF MF^C	205	-	0.2	-	Dead-end	1	327	Kaolin Ms	1.6	327	312	143	-	98.8	-	
GVWP MF^C	125	70	0.22	-	Dead-end	1	6378	5 mg/L HA (pH 10)	-	6378			1722	29	73	[43]
							7874	20 mg/L HA (pH 8)	-	7874	-	-	1496	6	81	
GVHP MF^C	125	75	0.22	-	Dead-end	1	7924	5 mg/L HA (pH 8)	-	7924	-	-	1981	16	75	
PSU ENM^L	178	-	-	1110	Cross-flow	1	16513	15 mg/L HA (pH 11)	~0.004	16513	-	51	69	60	99	[7]
PVDF ENM 1^L	86	87.2	4.78	163	Dead-end	1	23880*	100 ppm PS Ms	1	23880*	-	-	-	87	-	[49]
PVDF ENM 2^L	78	85.7	3.30	163	Dead-end	1	15590*	100 ppm PS Ms	1	15590*	-	-	-	91	-	
PLA ENM 1^L	180	31.4	2.3	≥ 900	Dead-end	0.75	78000	0.12 wt% TiO_2	0.01-0.5	58500**	25947*	107*	-	61.0*	-	[26]
PLA ENM 2^L	130	27.6	1.4	≥ 900	Dead-end	0.75	78000	0.12 wt% TiO_2	0.01-0.5	58500**	8463*	52*	-	84.3*	-	
PLA ENM 3^L	120	18.0	2.0	≥ 900	Dead-end	0.75	78000	0.12 wt% TiO_2	0.01-0.5	58500**	1002*	27*	-	85.6*	-	
PES MF^C	-	≈ 70	0.16	-	Dead-end	0.69	6783	2 mg/L HA	-	4680	3865	202	-	95	-	[12]
PVDF MF^C	125	≈ 70	0.22	-	Dead-end	0.69	5217	2 mg/L HA	-	3600	3600	159*	-	93*	-	
PCTE MF^C	25	13.8	0.22	-	Dead-end	0.69	4957	2 mg/L HA	-	3420	1565	155	-	87	-	
PSU ENM 9^L	213	81.7	3.06	720	Cross-flow	1	20563	15 mg/L HA (pH 11)	~0.004	20563	17540	232	834	63.9	95.9	This study
PSU ENM 10^L	89	80.8	2.82	760	Cross-flow	1	20269	15 mg/L HA (pH 11)	~0.004	20269	8036	188	643	70.9	96.8	
PES HPWP MF^C	137	70-84	0.45	-	Cross-flow	1	14761	15 mg/L HA (pH 11)	~0.004	14761	1120	106	216	77.6	98.5	

[1]L = lab-made membrane; C = commercial membrane; ENM = electrospun nanofiber membrane; PSU = polysulfone; PVDF = polyvinylidene fluoride; PES = polyethersulfone; UF = ultrafiltration; MF = microfiltration; PLA = poly (lactic acid).
[2]LMH = L/m^2.h
[3]PS = polystyrene; Ms = microparticles; HA = humic acid.
[4]The initial permeate flux for the membranes of this study corresponds to the HA permeate flux after 2.5 min of the filtration test.
*Estimated values taken from figures plotted in the corresponding reference; **Average value.

Supporting Information

Heat-treated optimized polysulfone electrospun nanofibrous membranes for high performance wastewater microfiltration

P. Arribas[1,2,*], M.C. García-Payo[2], M. Khayet[2,3,*], L. Gil [4]

[1]Campus of International Excellence, Moncloa Campus (UCM-UPM), Madrid (Spain).

[2]Department of Structure of Matter, Thermal Physics and Electronics, Faculty of Physics, University Complutense of Madrid, Avda. Complutense s/n, 28040, Madrid (Spain).

[3]Madrid Institute for Advanced Studies of Water (IMDEA Water Institute), Calle Punto Net Nº 4, 28805, Alcalá de Henares, Madrid (Spain).

[4]Genetics and Eco-Physiology Research Group, School of Forest Engineering, University Polytechnic of Madrid, Avda. Complutense s/n, 28040, Madrid (Spain).

* Corresponding authors: khayetm@fis.ucm.es; paulaarribas@ucm.es

Tel. +34-91-3944448; +34-91-3945185

Fax. +34-91-3945191

Figure S1 shows examples to understand the way to evaluate the damage of the membranes due to the heat post-treatment (HPT). As it can be observed in Fig. S1, almost the entire surface of some of the membranes after the HPT step was burned (Fig. S1-A, red color). These membranes could not be used in filtration. Other membranes had only few burned spots on the surface, making their surface heterogeneous and not desirable for filtration tests (Fig. S1-B, yellow color). Finally, some membranes did not show visual damage and were therefore good candidates to be used for water treatment (Fig. S1-C, green color).

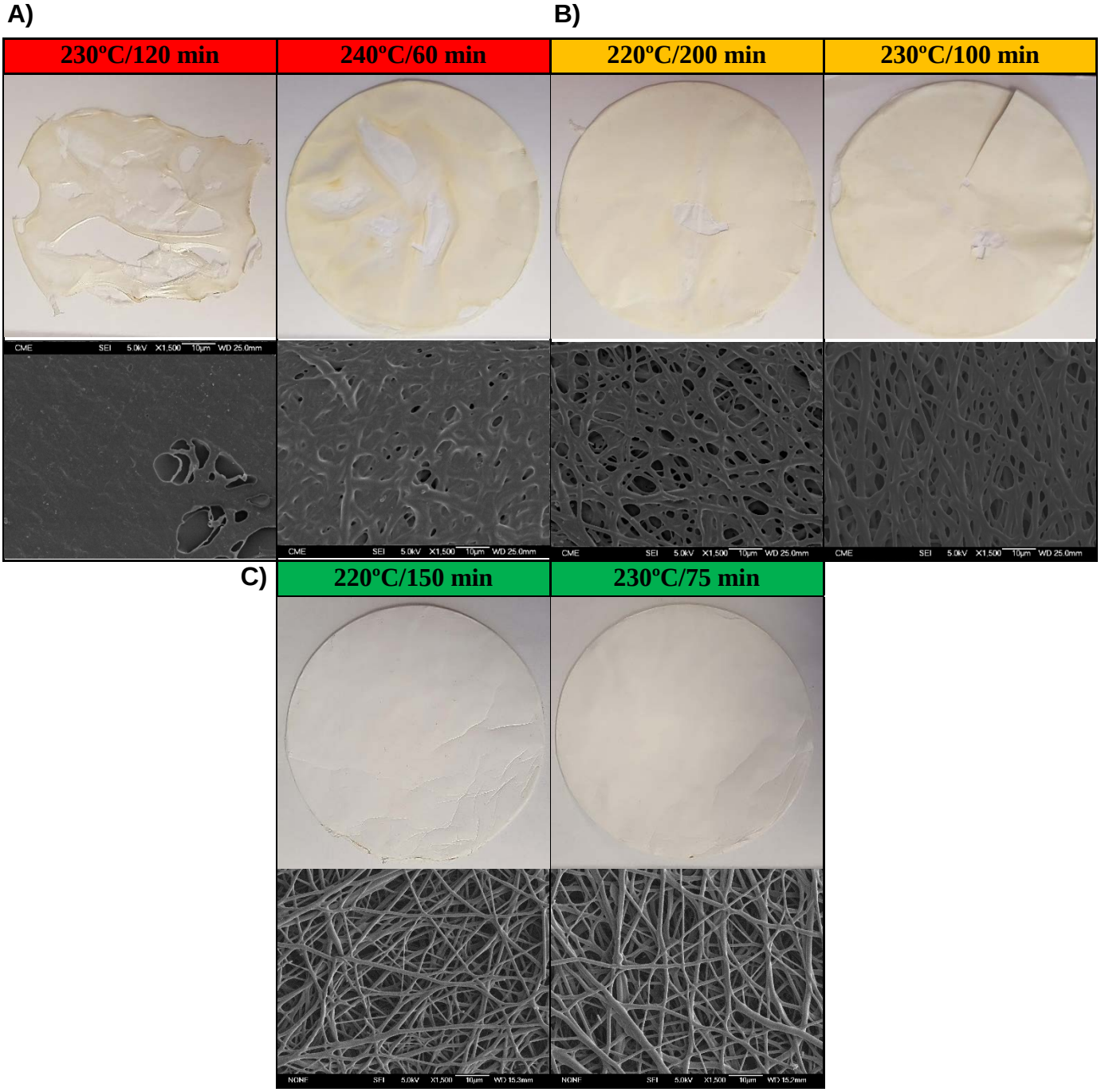

Fig. S1. Visual criterion to evaluate the damage of the membranes due to the HPT. Pictures of the PSU ENMs after the HPT (top) with their corresponding SEM image of the surface (bottom). A) Membranes graded with 0 points, B) 5 points and C) 10 points.

Figure S2 shows, as an example, how to evaluate the degree of networking and interconnectivity of the PSU ENMs after the application of the HPT. Firstly, the total number of the nanofibers intersections were quantified using their corresponding SEM surface images. Subsequently, the intersections in which the nanofibers are clearly fused together were identified. In this way, the degree of networking (*DN*) of each PSU ENM is given by the percentage ratio between these two values (i.e. *DN* = bonding points between nanofibers/total nanofibers intersections). Images of Fig. S2 show two examples of the nanofibers structure on the surface of PSU ENMs treated with a medium (230ºC/60 min) and a high (230ºC/75 min) HPT. The yellow circles represent some normal intersections between nanofibers while the red circles represent points with fused nanofibers, i.e. bonding points between nanofibers.

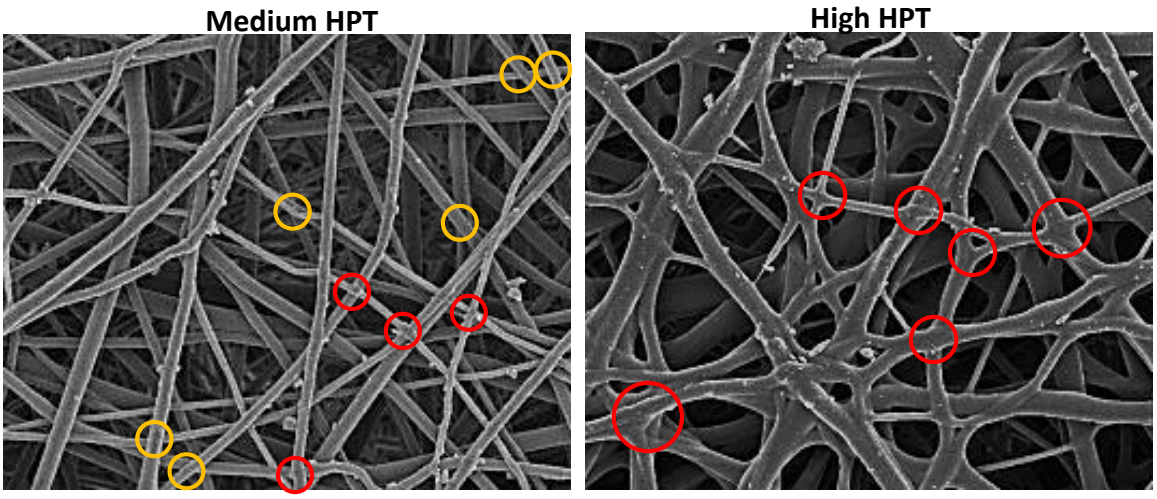

Fig. S2. Evaluation of the degree of networking and interconnectivity of the PSU ENMs after the application of the heat post-treatment (HPT). SEM images of the nanofibers structure on the surface of PSU ENMs treated with a medium (230ºC/60 min) and a high (230ºC/75 min) HPT. The yellow circles represent some normal intersections between nanofibers while the red circles represent points with fused nanofibers.

Figure S3 summarizes the nanofiber diameter distribution (i.e. nanofiber diameter histogram) of the treated PSU ENMs, obtained by statistical analysis applied on the nanofiber diameter measurements evaluated by UTHSCSA Image Tool 3.0 software.

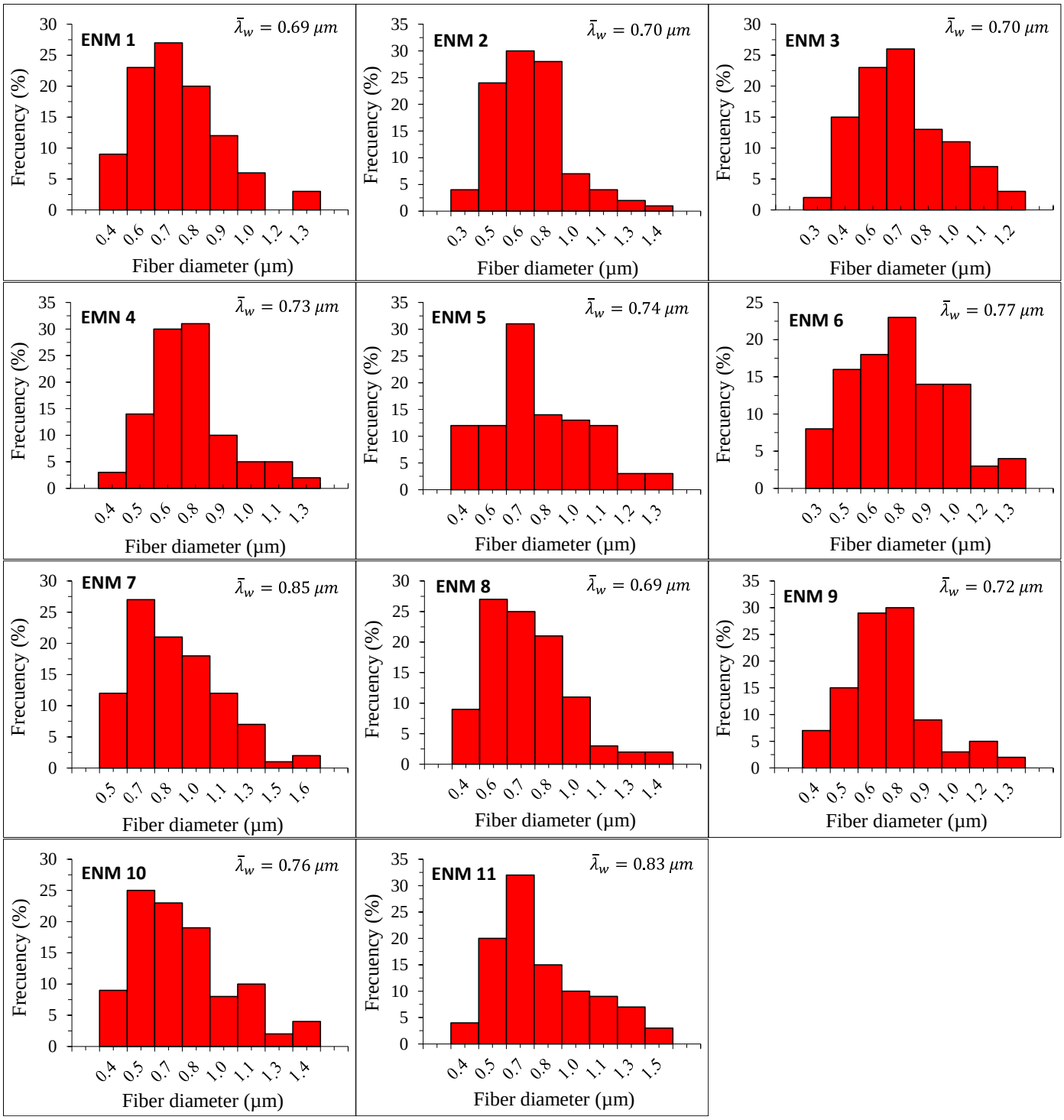

Fig. S3. Nanofibers diameter histograms of the treated PSU ENMs.

Figure S4 is a sketch showing the effects of the heat post-treatment (HPT) on the nanofiber diameters and the size of the inter-fiber space of the ENMs. ENMs after fabrication via electrospinning had a thickness of about 900 ± 50 μm. To carry out the HPT, the ENMs are attached to a copper support and introduced in a ceramic oven. After the HPT is completed, the thickness of the ENMs was reduced and varied in the range of 80-380 μm. One of the main effects observed with the increase of the HPT temperature or time was the increase of the nanofiber diameters ($\overline{\lambda_w}$) of the membranes along with a decrease of the mean size of the inter-fiber space ($\overline{d_f}$), i.e., nanofibers became flatter and thicker along the membrane, resulting in a decrease in the mean size of the inter-fiber space.

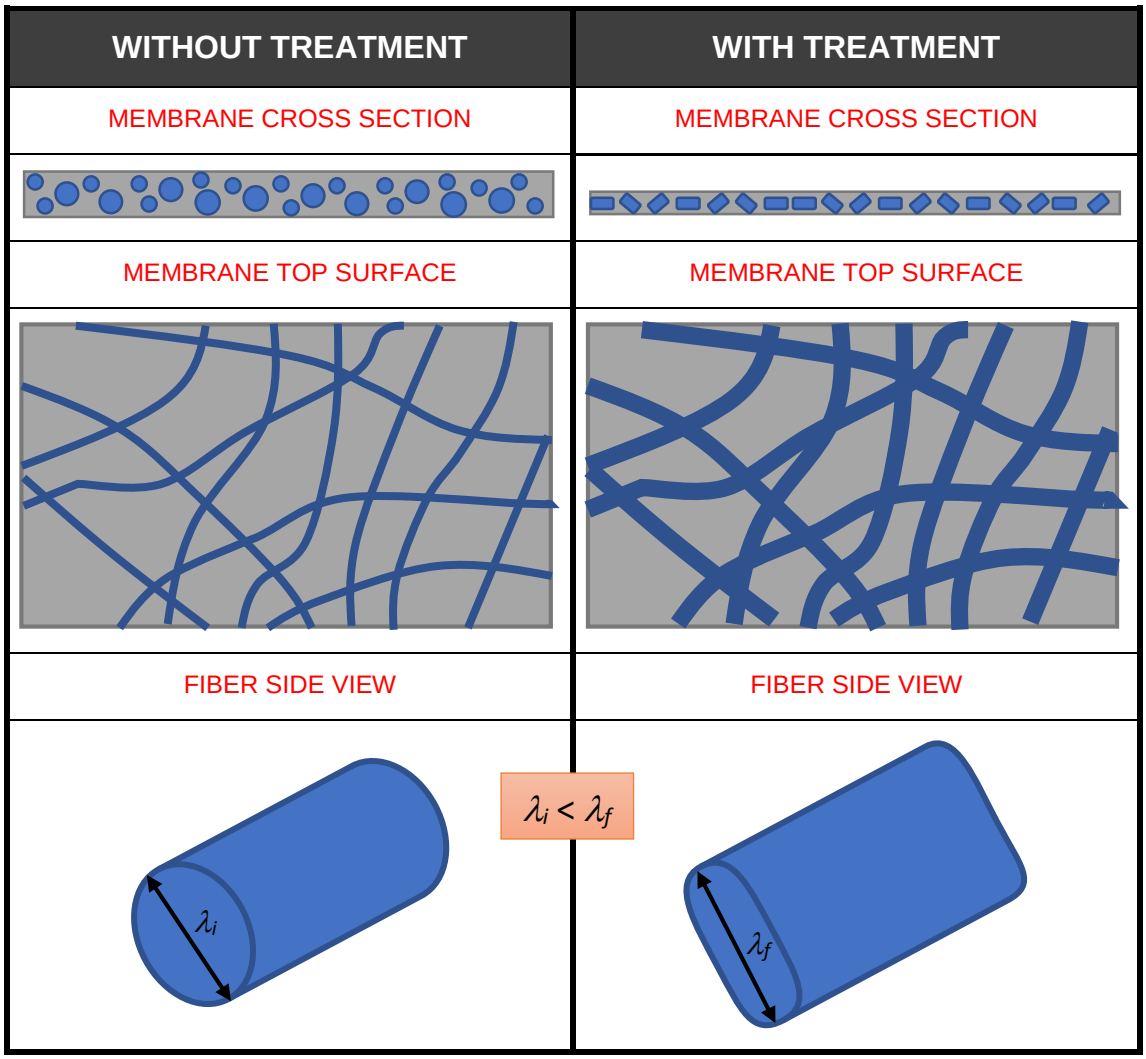

Fig. S4. Sketch of the effects of the heat post-treatment (HPT) on the nanofiber diameters and the size of the inter-fiber space of the ENMs. The parameters λ_i and λ_f represent the initial and final diameter of the nanofibers, respectively.

Figure S5 shows as an example some of the techniques used for the analysis of the fouling of the PSU ENMs. From the FTIR analysis (see Fig. S5-A) it can be observed the appearance of characteristic peaks of the humic acid (HA) on the spectra of the ENM after HA microfiltration (MF) (indicated with black arrows over the graph), what confirms the presence of HA in the membranes after filtration. The surface and the cross-section of the self-sustained PSU ENMs were examined by a field emission scanning electron microscope (FESEM, JEOL Model JSM-6330F) equipped with an energy-dispersive spectrometer (EDS, Oxford Instruments X-Max). The accumulation of HA on the surface of the ENMs can be observed from the SEM bottom image of Fig. S5-B. EDS in mapping mode together with the software INCA (Oxford Instruments) were used to determine the elemental composition of the ENMs before and after HA MF along the cross-section of the membrane samples. This elemental analysis was performed in three differentiate areas: the bottom side (i.e. facing the permeate), the center side and the top side (i.e. facing the feed). The cross section SEM images of Fig. S5-C correspond to the PSU ENM after HA MF. The elemental analysis areas are highlighted with a pink square over the cross section SEM images. The graph under these images summarizes the relative percentage (i.e. Element/C) of the atomic composition of the ENM before and after HA MF in the three areas of interest. Before HA filtration, the relative percentage concentration of sulfur (S/C) and oxygen (O/C) detected in the membrane was practically the same in the three areas of interest, i.e. there was a homogeneous distribution of these elements across the membrane. In addition, the concentration ratio of O/C across the membrane was higher than that of S/C, which is in concordance with the chemical formula of the PSU (i.e. $C_{27}H_{46}O_4S_1$). After HA filtration, a 13 to 25% decrease of the S/C ratio and a 7 to 22% increase of the O/C ratio across the membrane were observed as well as the emergence of new elements such as aluminum (Al), silicon (Si) and iron (Fe) coming from the HA. It is worth noting that the O/C ratio was higher in the top side (0.27) than that of the bottom and center sides (0.21 and 0.20, respectively), probably due to the higher accumulation of HA in the top side of the membrane. In the same way, the concentration ratio of the new elements (i.e. Al/C, Si/C, Fe/C) was not homogeneous across the membrane. Although the analysis shows that fouling occurs along the whole cross-section of the membrane, the accumulation of these elements increase in the order: bottom side<center side<top side, being the Al/C, Si/C and Fe/C concentration ratios 79, 84 and 100 % higher, respectively, in the top side than in the bottom side.

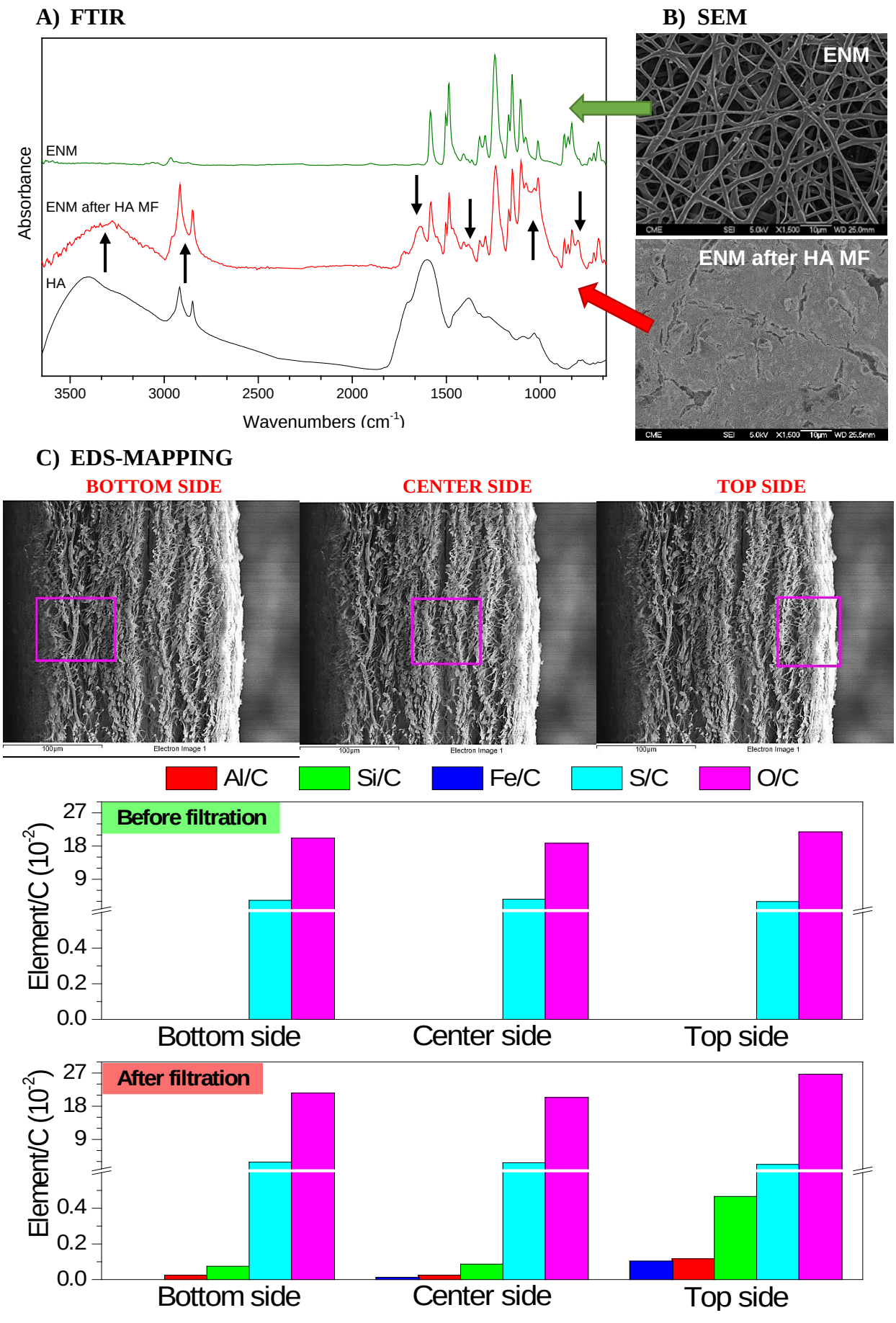
A) FTIR
B) SEM
ENM
ENM after HA MF
HA
Absorbance
3500
3000
2500
2000
1500
1000
Wavenumbers (cm-1)
ENM
ENM after HA MF
C) EDS-MAPPING
BOTTOM SIDE
CENTER SIDE
TOP SIDE
Al/C
Si/C
Fe/C
S/C
O/C
Before filtration
After filtration
Element/C (10-2)
27
18
9
0.4
0.2
0.0
Bottom side
Center side
Top side

Fig. S5. Example of the characterization analysis of the organic fouling of the PSU ENMs. A) FTIR spectra of the HA and the ENM before and after filtration. B) SEM surface images of the ENM before and after filtration (X1500). C) SEM cross section images of the ENM after filtration taken during the EDS mapping analysis in the bottom, centre and top sides of the membrane. The graph under the images summarizes the relative percentage (i.e. Element/C) of the atomic composition of the ENM before and after HA MF in the bottom, center and top sides.

Figure S6 shows the main results of the filtration parameters analyzed during the HA MF tests conducted with the treated-optimized PSU ENMs 9 and 10 (i.e. HPT of 230°C/60 min and 230°C/75 min, respectively) and the PES MF commercial membrane. SEM surface images of the membranes before HA MF test are included to realize the initial differences in the morphological structure of the membranes.

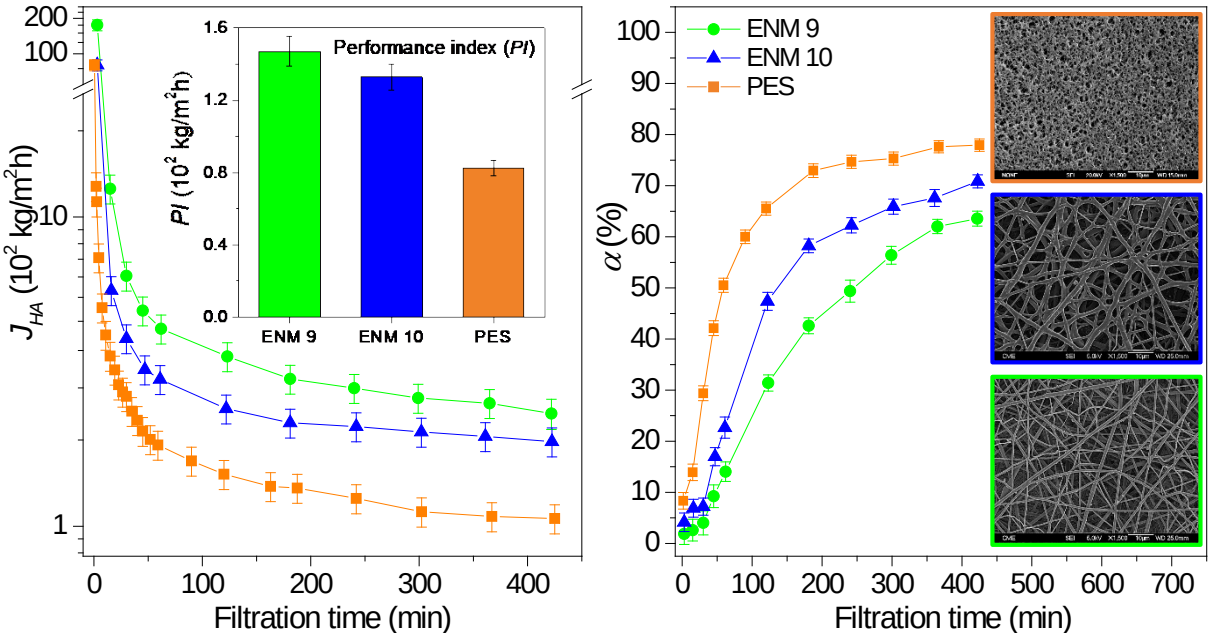

Fig. S6. Humic acid permeate flux (J_{HA}), separation factor (α) and performance index (PI) of the PSU ENMs 9 and 10 prepared with a HPT of 230°C/60 min and 230°C/75 min, respectively, and PES MF commercial membrane. The filtration tests were conducted with 15 mg/L HA feed aqueous solution at pH 11 and 10^5 Pa transmembrane pressure (ΔP). The inset pictures are SEM surface images of the membranes before HA MF test.